Cellular/Molecular

Thyroid Hormone Deficiency Affects Postnatal Spiking Activity and Expression of Ca^{2+} and K^+ Channels in Rodent Inner Hair Cells

Niels Brandt,[1]* Stephanie Kuhn,[1]* Stefan Münkner,[1] Claudia Braig,[2] Harald Winter,[2] Nikolaus Blin,[3] Reinhard Vonthein,[4] Marlies Knipper,[2] and Jutta Engel[1]

[1]Institute of Physiology II and Department of Otolaryngology, and [2]Department of Otolaryngology, Molecular Neurobiology, Tübingen Hearing Research Centre, University of Tübingen, D-72076 Tübingen, Germany, [3]Department of Molecular Genetics, Institute of Anthropology and Human Genetics, University of Tübingen, 72074 Tübingen, Germany, and [4]Department of Medical Biometry, University of Tübingen, 72070 Tübingen, Germany

Thyroid hormone (TH) is essential for the development of hearing. Lack of TH in a critical developmental period from embryonic day 17 to postnatal day 12 (P12) in rats and mice leads to morphological and functional deficits in the organ of Corti and the auditory pathway. We investigated the effects of TH on inner hair cells (IHCs) using patch-clamp recordings, capacitance measurements, and immunocytochemistry in hypothyroid rats and athyroid *Pax8*$^{-/-}$ mice. Spontaneous and evoked Ca^{2+} action potentials (APs) were present in control IHCs from P3–P11 rats and vanished in parallel with the expression of a rapidly activating Ca^{2+}- and voltage-activated K^+ (BK) conductance. IHCs of hypothyroid rats and athyroid *Pax8*$^{-/-}$ mice displayed APs until the end of the third postnatal week because of threefold elevated Ca^{2+} currents and missing expression of BK currents. After the fourth postnatal week, some IHCs showed BK currents whereas adjacent IHCs did not, demonstrated by electrophysiology and immunocytochemistry. To test whether the prolonged spiking activity during TH deficiency may be transmitted at IHC synapses, capacitance measurements were performed in parallel to analysis of otoferlin expression, a protein thought to play an essential role in exocytosis of IHCs. Strikingly, otoferlin was absent from IHCs of hypothyroid rats but not of *Pax8*$^{-/-}$ mice, although both cell types showed exocytosis with an efficiency typical for immature IHCs. These results demonstrate for the first time a TH-dependent control of IHC spiking activity before the onset of hearing attributable to effects of TH on Ca^{2+} and BK channels. Moreover, they question an indispensable role of otoferlin for exocytosis in IHCs.

Key words: **inner hair cell; thyroid hormone; BK channel; $Ca_v1.3$ channel; Ca^{2+} action potential; otoferlin**

Introduction

Thyroid hormone (TH) or triiodothyronine (T3) and its receptors are essential for the development of hearing. Congenital thyroid disorders impair hearing, and iodine deficiency causes profound deafness (Dussault and Ruel, 1987; DeLong, 1993; Forrest, 1996). Furthermore, hypothyroidism causes deformities in the organ of Corti and has indicated a critical window of TH requirement during inner ear development preceding the onset of hearing (Deol, 1973; Uziel, 1986; O'Malley et al., 1995; Knipper et al., 2000).

T3 receptors (TRs) are ligand-dependent transcription factors encoded by the related genes *TRα* and *TRβ* (Sap et al., 1986; Weinberger et al., 1986). Deletion or mutations of thyroid hormone receptor β (TRβ) cause hearing impairment or deafness in mice (Forrest et al., 1996) and humans (Refetoff et al., 1967; Brucker-Davis et al., 1996), whereas a role of TRα1 in hair cell differentiation has only recently emerged (Winter et al., 2006).

Hearing loss in TRβ-deficient mice was correlated with a severe retardation of a fast-activating potassium conductance, $I_{K,f}$, in the inner hair cells (IHCs) (Rusch et al., 1998). $I_{K,f}$ transforms the immature IHC into a sensory cell producing graded receptor potentials at the onset of hearing [around postnatal day 12 (P12)] (Kros et al., 1998). Before the upregulation of the rapidly activating Ca^{2+}- and voltage-activated K^+ (BK) channel underlying $I_{K,f}$ (Langer et al., 2003; Pyott et al., 2004; Hafidi et al., 2005), IHCs generate spontaneous Ca^{2+} action potentials (APs) despite lack of sensory input (Kros et al., 1998; Marcotti et al., 1999). This spontaneous activity triggers exocytosis (Beutner and Moser, 2001; Johnson et al., 2005), leads to EPSPs on the afferent nerve fibers (Glowatzki and Fuchs, 2002), and is thought to trigger maturation processes in the auditory pathway. Because Ca^{2+} APs rely on voltage-activated Ca^{2+} currents (Beutner and Moser, 2001; Marcotti et al., 2003b; Johnson et al., 2005), the consequences of deleting the predominant IHC Ca^{2+} channel $Ca_v1.3$ (Platzer et al., 2000), lack of Ca^{2+} APs and lack of BK channel

Received Sept. 12, 2006; revised Feb. 20, 2007; accepted Feb. 21, 2007.

This work was supported by University of Tüebingen Fortune Grant 1446-0-0 (J.E.) and Deutsche Forschungsgemeinschaft Grants En294/2-4,5 (J.E.) and Kni316/4-1 (M.K.). We thank Sylvia Kasperek and Karin Rohbock for excellent technical assistance, Hans-Peter Zenner for his continuous support, Karl Bauer for providing Pax8$^{+/-}$ mice, and Rama Panford-Walsh for discussion of this manuscript. This work is dedicated to the memory of Alfons Rüsch (1959–2002).

*N.B. and S.K. contributed equally to this work.

Correspondence should be addressed to Dr. Jutta Engel, University of Tübingen, Institute of Physiology II and Department of Otolaryngology, Tübingen Hearing Research Centre, Gmelinstrasse 5, D-72076 Tübingen, Germany. E-mail: jutta.engel@uni-tuebingen.de.

DOI:10.1523/JNEUROSCI.3965-06.2007

 0270-6474/07/273174-13$15.00/0

expression, indicate that Ca^{2+} APs also contribute to the differentiation of IHCs (Brandt et al., 2003).

Here, we investigated whether neonatal Ca^{2+} APs were affected by TH deficiency using two animal models: (1) *Pax8*$^{-/-}$ mice that show the most severe hypothyroid phenotype because of absence of thyroid follicular cells (Mansouri et al., 1998) and develop an inner ear phenotype typical for hypothyroidism (Christ et al., 2004), and (2) rat pups treated with methylmercapto-imidazol (MMI) during fetal and postnatal development, leading to hypothyroidism and deafness (Deol, 1973; Uziel, 1986; Knipper et al., 2000).

In both animal models, TH deficiency caused a prolongation of spiking activity because of a changed expression of $Ca_v1.3$ and BK currents. Capacitance measurements revealed robust exocytosis in TH-deficient IHCs in the entire phase of spiking activity. Strikingly, the IHC protein otoferlin (Yasunaga et al., 1999; Schug et al., 2006) was absent from hypothyroid rat IHCs at the mRNA and protein level, thus questioning the essential role of otoferlin for IHC exocytosis (Roux et al., 2006).

In a parallel study, Sendin et al. (2007) analyzed the effects of TH deficiency on the maturation of ion channels, presynaptic proteins, and exocytosis in *Pax8*$^{-/-}$ mice.

Materials and Methods

Animals. Hypothyroid Wistar rats (Charles River, Sulzfeld, Germany) and athyroid *Pax8*$^{-/-}$ mice (Mansouri et al., 1998) were used. Hypothyroidism in rats was induced by treating mothers and pups with methylmercapto-imidazol (Knipper et al., 2000). *Pax8*$^{-/-}$ mice were born from heterozygous Pax8$^{+/-}$ parents; their euthyroid littermates Pax8$^{+/-}$ and Pax8$^{+/+}$ (Mansouri et al., 1998; Christ et al., 2004) served as controls (here designated as *Pax8* control). Animals were killed by decapitation (after CO_2 anesthesia for ages older than P9) and cochleae were removed according to national ethical guidelines. Animal experiments were approved and undertaken in accordance with the protocol requirements of the University of Tuebingen.

Electrophysiological recordings. The IHCs of rats or mice were studied in acute preparations of the organ of Corti after the cell somata had been partially exposed with cleaning pipettes and positive or negative pressure. Spiking activity and whole-cell K^+ currents in IHCs younger than P12 were recorded in extracellular solution B1 [containing the following (in mM): 153 NaCl, 5.8 KCl, 1.3 $CaCl_2$, 0.9 $MgCl_2$, 0.7 NaH_2PO_4, 10 HEPES, 5.6 glucose, pH 7.4, 320 mOsm kg^{-1}]. For IHCs P12 or older, a solution with a reduced Cl^- concentration was used [B1-mature; containing the following (in mM): 85 NaCl, 70 lactobionate × NaOH, 5.8 KCl, 1.3 $CaCl_2$, 0.9 $MgCl_2$, 0.7 NaH_2PO_4, 10 HEPES, 5.6 glucose, pH 7.4, 320 mOsm kg^{-1}], which better preserved the organ of Corti and the IHCs (Siegel et al., 2001). The pipette solution I1 consisted of (in mM) 110 K-gluconate, 20 KCl, 10 Na^+ phosphocreatine, 5 HEPES, 5 EGTA, 4 $MgCl_2$, 4 Na_2ATP, 0.1 $CaCl_2$, and 0.3 GTP, pH 7.35, 305 mOsm kg^{-1}.

To isolate currents through Ca^{2+} channels from large K^+ (and neonatal Na^+) currents, 10 mM Ba^{2+} was used as a charge carrier, as well as a combination of intracellular and extracellular K^+-channel blockers. For IHCs younger than P12, the extracellular solution B2 consisted of (in mM) 160 tris-(hydroxy-methyl-amino)-methane × HCl, 10 $BaCl_2$, 5.6 glucose, and 1 $MgCl_2$, pH 7.4, 320 mOsm kg^{-1} (Michna et al., 2003). For IHCs P12 or older, B2-mature was used [containing the following (in mM): 70 lactobionate × NaOH, 40 NaCl, 35 tetraethylammonium chloride (TEA), 15 4-aminopyridine (4-AP), 10 $BaCl_2$, 10 HEPES, 5.6 glucose, and 1 $MgCl_2$, pH 7.4, 320 mOsm kg^{-1}]. The pipette solution for isolating Ba^{2+} currents, I2, was composed of (in mM) 120 Cs^+ gluconate, 20 CsCl, 10 Na^+ phosphocreatine, 5 HEPES, 5 EGTA, 4 $MgCl_2$, 4 Na_2ATP, 0.1 $CaCl_2$, and 0.3 GTP, pH 7.35, 305 mOsm kg^{-1} (Michna et al. 2003). All chemicals were obtained from Sigma (St. Louis, MO) with the exception of ATP, TEA, lactobionate (Fluka, Neu-Ulm, Germany), and iberiotoxin (Alomone Labs, Jerusalem, Israel).

Whole-cell recordings were performed from IHCs of the apical or medial cochlear turn (before P12) or of the apical cochlear turn (P12 or later) at room temperature (22°C) using the whole-cell patch-clamp technique in either current-clamp or voltage-clamp mode with an Axopatch 200B amplifier (Molecular Devices, Union City, CA). Patch pipettes with a resistance of 4–6 MΩ were pulled from quartz glass. Currents were corrected off-line for linear leak currents and voltages were corrected for the uncompensated series resistance and for liquid junction potentials [cf. Neher (1992), B1/I1 = −12.6 mV; B1-mature/I1 = −9.6 mV; B2/I2 = −20 mV; B2-mature/I2 = +2.3 mV, to be added to the respective voltages].

Data acquisition. Data were acquired using the software Pulse++ 1.7 (developed by Ulrich Rexhausen, Institute of Physiology II, Tuebingen, Germany, and Klaus Bauer, Max Planck Institute for Medical Research, Heidelberg, Germany) and an ITC16 interface (Instrutech, Greatneck, NY) and were stored on a Macintosh G3 computer (Apple, Cupertino, CA). Voltage traces lasting 10 s were sampled at 5 kHz and filtered at 1.3 kHz; short current traces lasting 30 ms were sampled at 100 kHz and filtered at 10 kHz, and longer current traces (500 ms) at 5 kHz/1.3 kHz.

Data analysis. Data analysis was performed using the Igor software package (Wavemetrics, Lake Oswego, OR) as described previously (Michna et al., 2003); statistical analysis was done with JMP IN 5.1 Software (SAS Institute, Cary, NC). CV denotes coefficient of variation and R^2 the coefficient of determination.

A transient voltage change was considered as an action potential when its peak was ≥10 mV positive from the resting potential and its width was <100 ms. How frequently spontaneous and induced spiking occurred at different ages in the two rat groups (control vs hypothyroid) was quantified by logistic regression on covariables age, exp(age), factor MMI treatment, and the group–exp(age) interaction. For *Pax8* control and *Pax8*$^{-/-}$ mice, a simpler model without exponential function and interaction sufficed. The maximum spiking frequency of an IHC was determined as the maximum frequency at which the cell could generate Ca^{2+} APs, either spontaneously or induced, by increasing injections of current before the membrane potential became arrested in a depolarized state. Resting membrane potentials were determined as average membrane potentials in nonspiking cells. In spontaneously active cells, resting potentials were determined using the voltage of the lower peak of the voltage histogram (bin width, 0.5 mV) in a 10 s recording episode. The membrane potential as a function of postnatal age and MMI treatment was modeled by a four-parameter logistic curve with different ages of half-maximal decrease for the control and the MMI-treated group. Parameters of this nonlinear regression were estimated by the least squares method. Peak current–voltage (*I–V*) curves of K^+ currents (I_K) were determined using a peak search routine and by averaging I_K in a 2 ms window centered around the time of peak for each voltage (i.e., these currents were determined not necessarily at the same time point of the voltage-induced current responses). In contrast, *I–V*s for Ba^{2+}/Ca^{2+} currents and for the fast component of I_K were determined at fixed time points (averaged for the following millisecond) at every voltage, as indicated in the respective figures and legends. Activation time constants of K^+ currents were determined by monoexponential fits to the current traces for either 2 ms (when currents activated rapidly) or 7 ms (when only slowly activating currents were present).

The age-dependent rise of peak K^+ currents in *Pax8* mice was described by analysis of covariance (ANCOVA) of logarithms to obtain constant variance. A group–age interaction allowed for different slopes. Variance of logarithms of exocytosis efficiency was explained (ANOVA) by factors group, age (where applicable), stimulus duration, all of their interactions, and random cell effects.

Data are given as mean ± SD except in Figures 8*C–F* and 9*B*,*C* (mean ± SEM), and Figures 7*C*, 8*G*,*H*, and 9*D*, where median values are presented and some 95% confidence intervals (CIs).

Capacitance measurements. To analyze exocytosis, we measured increases in the membrane capacitance after voltage steps of different durations, which lead to fusion of synaptic vesicles with the plasma membrane (Neher and Marty, 1982). The "track-in" mode of the Optopatch amplifier (Cairn Research, Faversham, UK) was used where a self-balancing lock-in amplifier is integrated into the patch-clamp circuitry, detecting and compensating changes of membrane resistance and membrane capacitance in real-time (Johnson et al., 2002). IHCs were placed in

B1 (before P12) or B1-mature solution (P12 or later) and superfused with a solution containing 5 mM Ca^{2+} and K^+-channel blockers [B3; containing the following (in mM): 110 NaCl, 5 $CaCl_2$, 1 $MgCl_2$, 5.6 glucose, 10 HEPES, 35 TEA, and 15 4-AP, pH 7.4, 320 mOsm kg^{-1}]. Ca^{2+} dependence of exocytosis was tested with a nominally Ca^{2+}-free superfusion (B4, for which solution B3 was modified by replacing 5 mM $CaCl_2$ with 1 mM $MgCl_2$ and 10 mM NaCl). The pipette solution for measuring changes in membrane capacitance, I3, corresponded to I2 (see above) except that Cs^+ methane sulfonate (105 mM) replaced Cs^+ gluconate (120 mM).

At a holding potential of −80 mV, a sine wave (frequency, 0.9–1.2 kHz) was applied to the IHC with an amplitude small enough (10–20 mV rms) to avoid significant changes in membrane conductances, which was interrupted by a single voltage step from −80 to 0 mV to trigger Ca^{2+} influx and exocytosis. The resulting capacitance change (ΔC_m) was calculated as the difference of the mean capacitance over 300 ms after depolarization (the first 100 ms were skipped) (Moser and Beutner, 2000) and the mean prepulse capacitance (300 ms). Voltage steps with different durations (5, 10, 20, 40, 80, and 100 ms) were applied in random order.

Immunocytochemistry. For whole-mount immunocytochemistry of BKα, the cochlea was injected with 2% paraformaldehyde for 15 min on ice, rinsed with PBS, and the external bone was removed. The modiolus with the organ of Corti attached was stained as described for cochlear cryosections (Knipper et al., 1998, 2000). Antibodies against BKα (Alomone Labs) and neurofilament NF200 (The Binding Site, Heidelberg, Germany) were used. For otoferlin staining, cochlear cryosections were used for which cochleae older than P9 were decalcified for 1–5 min with Rapid Bone Decalcifier (Fisher Scientific, Houston, TX). Otoferlin antibodies were generated by immunizing a rabbit (Pineda, Berlin, Germany) with three synthetic peptides (amino acids 238–263, 1296–1317, 1370–1384; GenBank accession number AF183183) of mouse otoferlin (Schug et al., 2006). The antibody was purified against the amino acids 1370–1384, and specificity was tested by blocking with the specific peptide. Primary antibodies were detected with Cy3-conjugated (Jackson ImmunoResearch, West Grove, PA) or Alexa Fluor 488-conjugated antibodies (Invitrogen, Eugene, OR). Specimens were embedded with Vectashield mounting medium containing 4,6,diamidino-2-phenylindole (DAPI) (Vector Laboratories, Burlingame, CA) to stain cell nuclei (blue) and viewed using an Olympus (Tokyo, Japan) AX70 microscope equipped with epifluorescence illumination. Staining was detected in at least three specimens of at least three animals.

Riboprobe synthesis and in situ *hybridization.* To generate an otoferlin-specific riboprobe (Schug et al., 2006), a 634 bp PCR fragment of otoferlin was amplified by reverse transcriptase-PCR using GoTaq DNA polymerase (Promega, Mannheim, Germany) with the primers 5′-gcttcctgcctaccctcgg-3′ and 5′-cagcttgtcagcaatgtgatcc-3′ from rat cochlear cDNA. The PCR product was sequenced and otoferlin specificity was confirmed. The fragment was cloned into the pCRII-Topo Vector (Invitrogen) and used for *in vitro* transcription. Complementary strands for sense and antisense were transcribed from either SP6 or T7 promoter sites in the presence of digoxigenin (DIG)-labeling mix (Roche Diagnostics, Mannheim, Germany).

In situ hybridization (ISH) was performed as described previously (Knipper et al., 1998). Briefly, DIG-labeled antisense or sense probes were diluted in hybridization solution containing 25% microarray hybridization buffer (GE Healthcare, Freiburg, Germany), 25% nuclease free water, and 50% formamide. Sections were stained by an anti-DIG-antibody coupled to alkaline phosphatase for 20 h.

Results

Effects of TH deficiency on spiking activity in rat IHCs

The organs of Corti of postnatal hypothyroid rats were characterized by an immature morphology and an altered "sticky" extracellular matrix. Exposure of IHC somata was more difficult than in controls, leading to lower success rates of whole-cell recordings.

Spontaneous oscillations of the membrane potential occurred in neonatal IHCs, independent of the TH level from P3 onwards

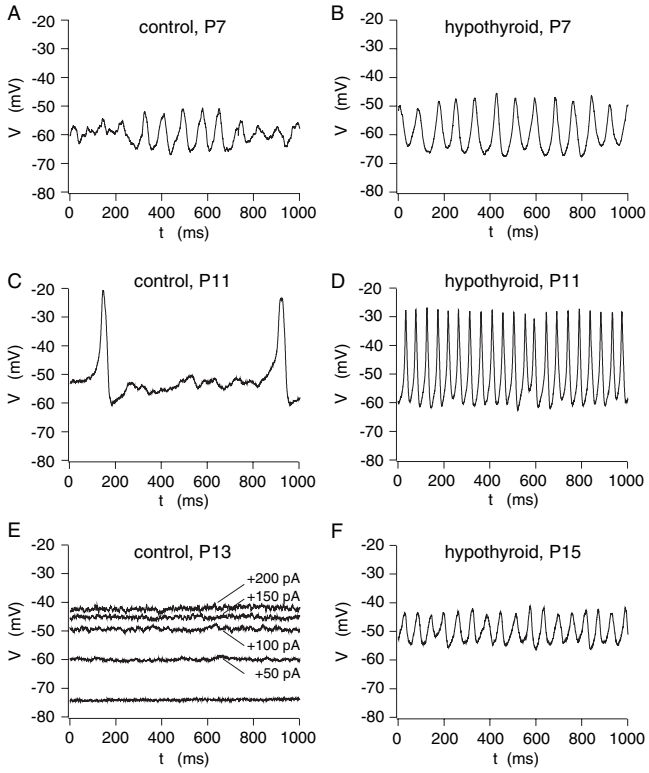

Figure 1. Postnatal IHCs of euthyroid and hypothyroid rats generate spontaneous Ca^{2+} action potentials. Membrane potentials of IHCs were recorded in the current-clamp mode ($I = 0$) of the whole-cell patch-clamp configuration. ***A***, ***B***, Spontaneous action potentials in P7 IHCs of control rats (***A***) were similar to those of hypothyroid rats (***B***). ***C***, ***D***, At P11, a control rat IHC generated APs at low frequencies (2 Hz, ***C***) whereas, in contrast, a hypothyroid IHC showed spontaneous APs at a much higher rate (21 Hz, ***D***). ***E***, A control IHC did not show spontaneous spiking activity at P13 (lowermost trace) and current injections of 50–200 pA shifted the membrane potential in the positive direction (size of injected currents indicated at the traces) rather than triggering action potentials. ***F***, High-frequency spontaneous voltage oscillations (APs) persisted in an IHC of a hypothyroid rat at P15.

shown for control and hypothyroid rats at P7 (Fig. 1*A*,*B*). These action potentials (Ca^{2+} APs) depended on the presence of extracellular Ca^{2+} (data not shown) and resembled the Ca^{2+} APs studied in neonatal mouse IHCs (Kros et al., 1998; Marcotti et al., 1999, 2003b, 2004b). Rapidly activating and deactivating Na^+ currents were present in <20% of control and hypothyroid IHCs, indicating that Na^+ currents were not necessary for the generation of Ca^{2+} APs. Their amplitude was rather small at P7 (Fig. 1*A*) when they looked like symmetric voltage oscillations, and increased toward P11, when all IHCs tested displayed spontaneous Ca^{2+} APs (Fig. 1*C*,*D*). The spiking frequency of hypothyroid IHCs exceeded by far the frequencies observed in control IHCs of the same age (Fig. 1*C*,*D*). By P13, spontaneous Ca^{2+} APs had completely vanished in control IHCs that displayed quite negative resting potentials of −70.1 ± 3.3 mV ($n = 5$). Injection of positive current led to gradual shifts of the membrane potential in the positive direction rather than eliciting any Ca^{2+} APs (Fig. 1*E*), indicating the successful transition from a neonatal spiking pacemaker to a mature IHC capable of graded transmitter release (Kros et al., 1998). In contrast, IHCs of hypothyroid rats of the same age continued to generate high-frequency Ca^{2+} APs, shown here for P15 (Fig. 1*F*), yet with reduced amplitudes.

At P19, the IHCs of both control and hypothyroid animals did not spike spontaneously anymore. In hypothyroid IHCs, but not in control IHCs, Ca^{2+} APs could be evoked by injection of small

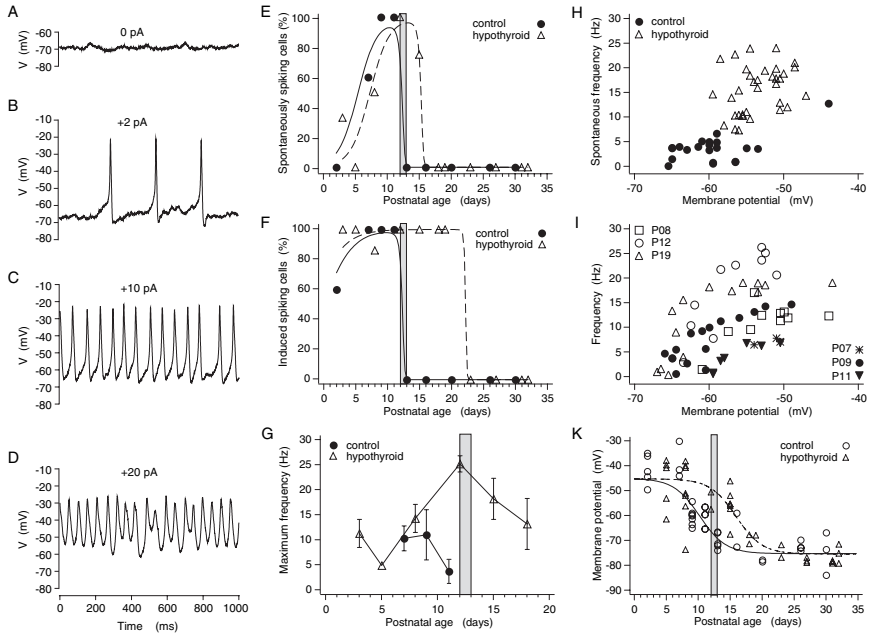

Figure 2. Spontaneous and induced spiking activity persist in IHCs of hypothyroid rats beyond P12. Electrically silent IHCs of both control and hypothyroid rats could be turned into electrically active cells by injecting small currents as shown for a hypothyroid IHC at P19 (***A–D***). ***A***, No spontaneous action potentials were present at a resting membrane potential of about −67 mV. ***B–D***, Ca^{2+} action potentials with increasing frequencies could be evoked by injections of small currents (2–20 pA as indicated at the traces). ***E***, Percentage of spontaneously active IHCs as a function of age for control and hypothyroid rats and logistic fits (solid line, control; dashed line, hypothyroid). ***F***, Percentage of electrically active IHCs as a function of age for control and hypothyroid animals and logistic fits (solid line, control; dashed line, hypothyroid). By injecting small currents, APs could be elicited in IHCs previously judged "electrically silent." Note that IHCs of control rats did not spike after P12, regardless of current injection (compare Fig. 1*E*). Numbers of IHCs in ***E***, ***F***: control, P2, 5; P7, 5; P9, 7; P11, 6; P13, 5; P16, 2; P20, 2; P26, 4; P30, 4; hypothyroid, P3, 6; P5, 6; P8, 8; P12, 2; P15, 8; P18, 2; P19, 1; P23, 2; P27, 3; P31, 3; P32, 3. ***G***, Average maximum frequencies for evoked APs in IHCs of hypothyroid and euthyroid rats as a function of age. Maximum spiking frequencies nearly doubled in hypothyroid IHCs at P12 or later compared with P8 hypothyroid or P7–P11 euthyroid (control) IHCs. IHC numbers: control, P7, 3; P9, 7; P11, 3; hypothyroid, P3, 2; P5, 1; P8, 5; P12, 2; P15, 6; P18, 3. ***H***, Dependence of the spontaneous frequency of Ca^{2+} APs on the membrane potential in control and hypothyroid IHCs. ***I***, Frequency-to-voltage curves for three typical control IHCs (filled symbols and asterisks) and hypothyroid IHCs (unfilled symbols) after current injection. Symbols and current sizes: asterisk, control, P7, from −54 to −45 pA; filled circle, control, P9, from −4 to 100 pA; filled triangle, control, P11, from 0 to 50 pA; unfilled rectangle, hypothyroid, P8, from −25 to 0 pA; unfilled circle, hypothyroid, P12, from −16 to 10 pA; unfilled triangle, hypothyroid, P19, from 2 to 35 pA. ***K***, Membrane potential values of rat IHCs and fits by a four-parameter logistic function of postnatal age with equal asymptotes and slopes and different times of half-maximal shifts for control (solid line) and hypothyroid rats (dashed line). The gray bars in ***E–G*** and ***K*** indicate the approximate age of the onset of hearing in control animals.

positive currents (2–20 pA), shown for a hypothyroid IHC at P19 (Fig. 2*A–D*). When comparing the spontaneous Ca^{2+} APs in IHCs as a function of age (Fig. 2*E*), relevant differences in the time period in which Ca^{2+} APs can be induced (Fig. 2*F*) and the maximal spiking frequency of IHCs (Fig. 2*G*) in control and hypothyroid animals can be observed. Whereas control IHCs never did spike spontaneously after P12, hypothyroid IHCs showed Ca^{2+} APs until P15 (Fig. 2*E*). Logistic regression confirmed later cessation of spontaneous spiking in hypothyroid IHCs. Current injections increased the percentage of spiking control IHCs only from P2 to P5 (Fig. 2*F*). From P12 onwards, no more Ca^{2+} APs could be elicited. In hypothyroid IHCs, the percentage of spiking cells could be increased by current injections from P3 to P8 and P15 to P19. Again, logistic regression revealed relevant differences in the termination of induced spiking between both animal groups. It has to be noted that before P7, only negative current injections of −10 to −40 pA could trigger Ca^{2+} APs, because of the depolarized potential of both control and hypothyroid IHCs (see below).

Another striking difference between IHC properties of control and hypothyroid rats was the maximum spiking frequency achieved in either spontaneous or evoked Ca^{2+} APs. The average maximum frequencies of Ca^{2+} APs in control IHCs shortly before the onset of hearing were ~10 Hz at P7 and P9 and dropped to <5 Hz at P11 (Fig. 2*G*). At P7, the IHCs of hypothyroid rats displayed average maximum frequencies of Ca^{2+} APs that were comparable with control IHCs but increased to values as high as 25 Hz at P12. Thereafter, maximum frequencies declined, but were still elevated compared with the highest values of control IHCs achieved at P9. Analysis of the dependence of spike frequencies on the resting membrane potential revealed differences for IHCs from control and hypothyroid rats (Fig. 2*H*,*I*) (for determination of the resting potential, see Material and Methods). Spontaneous Ca^{2+} APs of control IHCs with frequencies up to 7 Hz were generated from resting potentials of −65 to −53 mV (with one exception: −44 mV, 12 Hz) whereas those of hypothyroid IHCs with frequencies from 7 to 24 Hz arose from resting potentials of −60 to −47 mV (Fig. 2*H*). Current injections were able to induce Ca^{2+} APs and increased their frequencies as shown in Figure 2*I* for typical control (filled symbols, asterisk) and hypothyroid IHCs (unfilled symbols) of different ages. They increased the spiking frequency and shifted the membrane potential in the positive direction until IHCs stopped spiking and adopted a depolarized state. Whereas the control IHCs (filled symbols and asterisk) and the P8 hypothyroid IHCs (unfilled rectangle) showed frequency-resting potential relationships with similar steepness, those of P12 and P19 hypothyroid IHCs displayed much steeper curves (unfilled circles and triangles), suggesting a different ratio between depolarizing and repolarizing conductances. Finally, the resting membrane potentials of control and hypothyroid IHCs were compared (Fig. 2*K*), which shifted from about −40 mV after birth to about −75 mV at the end of the fourth postnatal week in both control and hypothyroid IHCs. Under the assumption of equal upper and lower asymptotes of the logistic curves, the fit resulted in residual SD of 7.2 mV or of $R^2 = 74\%$ of total variance of 72 observations. The half-maximal membrane potential change from newborn to mature occurred at P16 in hypothyroid rats and P10 in controls (difference, 5.6 d, SE, 0.12 d) (Fig. 2*K*).

Effects of TH deficiency on Ca^{2+} currents in rat IHCs

The persistence of high-frequency Ca^{2+} APs in the IHCs of hypothyroid rats beyond the onset of hearing of control animals raises the question about differences in the underlying conductances. Regenerative Ca^{2+} APs are based on the interplay of the negatively activating $Ca_v1.3$ Ca^{2+} channel and a slowly activating delayed rectifier-type K^+ channel (Muenkner et al., 2002). In normally developing mouse IHCs, Ca^{2+} APs cease when the BK conductance is expressed (Kros et al., 1998). In parallel, the

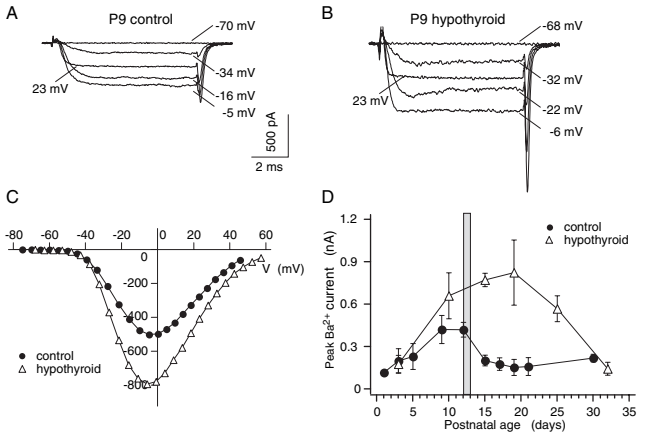

Figure 3. Ca^{2+} channel currents (charge carrier, 10 mM Ba^{2+}; I_{Ba}) in IHCs of hypothyroid rats showed a larger developmental I_{Ba} maximum and a delayed reduction of I_{Ba} to the mature levels of control IHCs. ***A***, ***B***, Selected I_{Ba} inward-current traces in response to step depolarizations for 8 ms of an IHC of a control rat (***A***) and of a hypothyroid rat (***B***) at P9, respectively. Command potentials are given at the traces, the holding potential was −70 mV (***A***) and −68 mV (***B***). ***C***, Corresponding current-voltage relations for the IHCs of the control and the hypothyroid rat were determined by averaging the current responses during the last millisecond of the voltage steps, respectively. ***D***, Peak I_{Ba} amplitudes were averaged for control and hypothyroid IHCs and plotted as a function of age. IHC I_{Ba} amplitudes of euthyroid controls showed a developmental maximum around P9 to P12 and a decline at ages older than P12 to values as low as in neonatals. Average I_{Ba} amplitudes in IHCs of hypothyroid rats showed a delayed maximum around P19 that was twice as large as in the control IHCs. *n* values: control IHCs, P1, 1; P3, 2; P5, 14; P9, 3; P12, 7; P15, 13; P17, 10; P19, 3; P30, 6; hypothyroid, P3, 2; P10, 7; P15, 2; P19, 6; P25, 4; P32, 2. The gray bar in ***D*** indicates the approximate age of the onset of hearing in control animals.

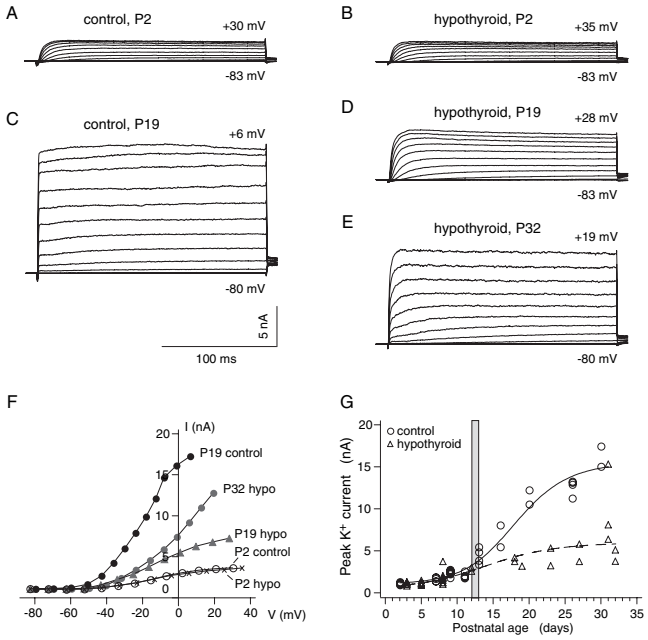

Figure 4. Peak K^+ current amplitudes remain smaller in IHCs of hypothyroid rats compared with controls until at least P32. ***A–E***, Whole-cell outward currents in postnatal IHCs of control and hypothyroid rats. ***A***, ***B***, Outward K^+ currents in neonatal IHCs (P2) of a control rat (***A***) and a hypothyroid rat (***B***) in response to 10 mV depolarization steps for 200 ms looked very similar. The holding potential and the maximum potential achieved are indicated below and above the traces, respectively. ***C***, Peak K^+ currents in a P19 control IHC increased by a factor of six during maturation and current activation became faster. ***D***, Outward currents in a P19 IHC of a hypothyroid animal were much smaller than in the P19 control IHC (***C***) and showed the same slow K^+-current activation kinetics as in the control and hypothyroid IHCs at P2 (***A***, ***B***). ***E***, In a P32 hypothyroid IHC, K^+ currents had further increased and showed faster activation kinetics compared with the hypothyroid IHC at P19 (***D***), but had not yet reached the amplitude and the fast kinetics of the K^+ currents of the P19 control IHC (***C***). ***F***, Peak *I–V*s of the whole-cell currents shown in ***A–E***. K^+ currents of P19 control IHCs were activating more negatively than P2 control IHCs and hypothyroid IHCs of every age. ***G***, Peak K^+ current amplitudes at 0 mV of 39 control and 40 hypothyroid IHCs as a function of age and four-parameter logistic regressions (solid line, control; dashed line, hypothyroid) applied to logarithms of K^+ currents with differences between hypothyroids and controls in every parameter. The curves are different ($p = 6.7 \times 10^{-9}$). The gray bar indicates the approximate age of the onset of hearing in control animals.

$Ca_v1.3$ conductance peaking at ~P6 declines (Beutner and Moser, 2001; Marcotti et al., 2003b). We first analyzed IHC Ca^{2+} currents in control and hypothyroid rats by using 10 mM Ba^{2+} as the charge carrier.

Figure 3*A*,*B* shows representative Ba^{2+} current (I_{Ba}) traces that were evoked by step depolarizations for 8 ms. Both control and hypothyroid IHCs showed rapidly activating and deactivating inward currents that did not inactivate. *I–V* curves calculated by averaging the current during the last millisecond of the voltage step and plotting it as a function of voltage revealed a larger I_{Ba} in the hypothyroid IHC compared with the control IHC at P9, with similar voltage dependence of I_{Ba} in the control and the hypothyroid IHC (Fig. 3*C*). Peak-current amplitudes were determined for both IHC groups for different ages. I_{Ba} of control rat IHCs showed a postnatal upregulation and downregulation with a peak amplitude between P9 and P12 and a subsequent downregulation to smaller values (40% of the peak) (Fig. 3*D*). This effect was comparable with the upregulation and downregulation in mouse IHCs, in which the peak occurs 3–4 d earlier (P6) (Beutner and Moser, 2001; Marcotti et al., 2003b). IHCs of hypothyroid rats at P3 had the same low I_{Ba} values, but from P10 onwards adopted values much larger than those of control IHCs, reaching an average of 824.9 ± 231 pA at P19, which corresponds to 180% of the peak values of the control at P9 and P12. At P24, I_{Ba} was still higher than the maximum values in control IHCs, and only at P32 I_{Ba} showed the same small I_{Ba} values as mature control IHCs.

These data demonstrate remarkably increased Ca^{2+} channel currents in IHCs of hypothyroid rats, strongly suggesting that TH is involved in the developmental downregulation of the Ca^{2+} conductance. Moreover, the elevated Ba^{2+}/Ca^{2+} current amplitudes favor the occurrence of Ca^{2+} APs seen in hypothyroid IHCs as long as the K^+ conductances are sufficiently large to repolarize the cell. Otherwise, the membrane potential would become arrested in a depolarized state. We therefore analyzed whole-cell K^+ currents as a function of age (Fig. 4).

Effects of TH deficiency on K^+ currents in rat IHCs

Whole-cell K^+ currents (I_K) elicited by step depolarizations were similar in neonatal control and hypothyroid IHCs as shown for P2 (Fig. 4*A*,*B*). At P19, the peak I_K amplitude of a control IHC had increased sixfold compared with that at P2 and also showed faster activation kinetics (Fig. 4*C*), which is consistent with the expression of the fast BK current (Kros et al., 1998; Langer et al., 2003; Marcotti et al., 2003a; Pyott et al., 2004). An age-matched IHC from a hypothyroid rat (P19) (Fig. 4*D*) showed much smaller K^+ currents with kinetics similar to those of the P2 hypothyroid IHC, but with a doubled peak amplitude. K^+ currents of a P32 hypothyroid IHC showed increased amplitudes and accelerated activation kinetics, but were still smaller than those of the P19 control IHC (Fig. 4*E*). The differences between I_K amplitudes of control and hypothyroid IHCs are further illustrated by the corresponding peak current *I–V* curves, in which the respective maxima of each current trace were plotted as a function of the membrane potential (Fig. 4*F*). Figure 4*G* summarizes peak I_K amplitudes as a function of age in control and hypothyroid IHCs:

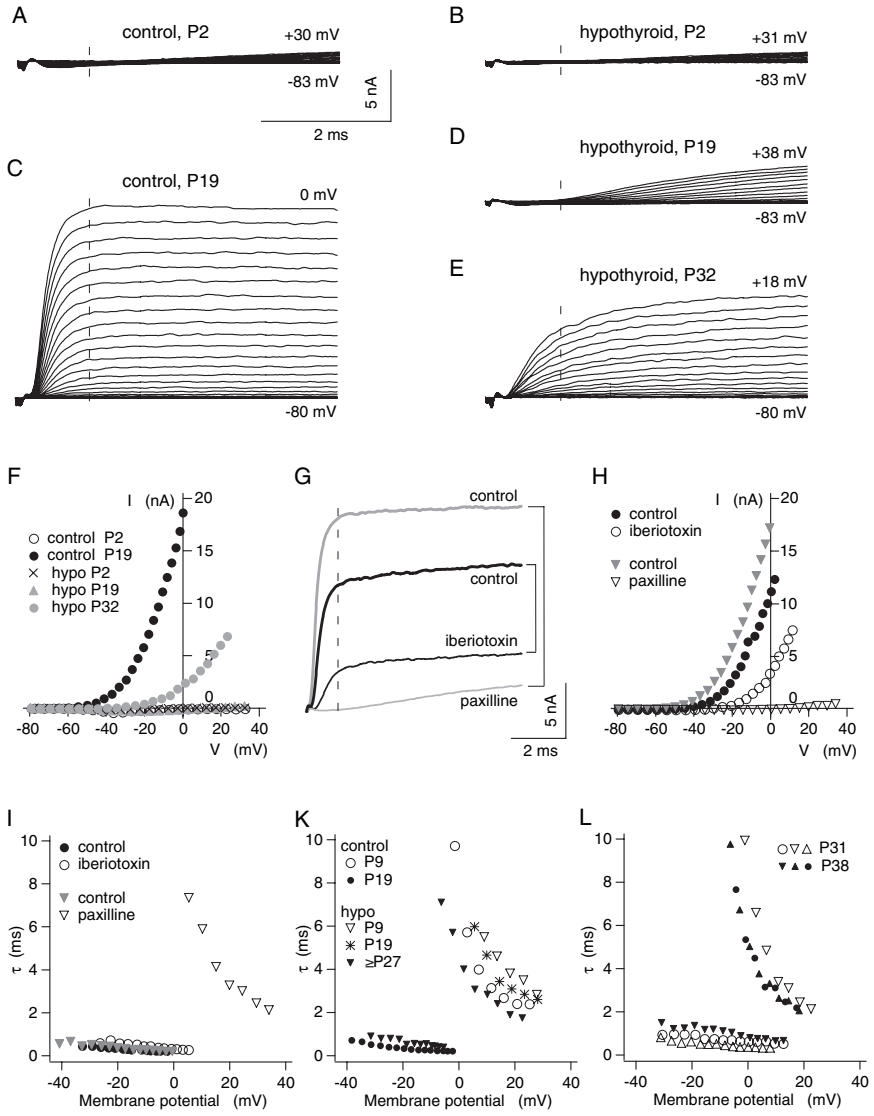

Figure 5. IHCs of hypothyroid rats do not acquire the fast BK conductance in the third postnatal week as IHCs of control rats do. ***A***, ***B***, Families of IHC outward K^+ current traces of a control rat (***A***) and a hypothyroid rat (***B***) at P2 in response to step depolarizations reveal similar slow activation kinetics within the first 5 ms. ***C***, In a P19 control IHC, a very large and rapidly activating K^+ current was evident. ***D***, ***E***, Expression of the rapidly activating conductance was missing in a hypothyroid IHC at P19 (***D***) and was still incomplete in another hypothyroid IHC at P32 (***E***). ***F***, *I–V*s of the K^+ currents in ***A–E*** taken at 1.2 ms after the start of the depolarization (the time point is indicated by vertical dashed lines in ***A–E***, respectively). IHCs of the P2 control rat and of either the P2 or P19 hypothyroid animals did not show any fast K^+ outward current within the whole voltage range whereas the P19 control IHC displayed a large and fast K^+ current. The P32 hypothyroid IHC showed some rapidly activating current. ***G***, Incomplete block of the fast K^+ current at 0 mV of a P19 control IHC (thick black trace) by the BK channel blocker iberiotoxin (100 nM, thin black trace) and complete block of the fast K^+ current at 0 mV of another P19 control IHC (thick gray trace) by the BK channel blocker paxilline (10 μM, thin gray trace). ***H***, *I–V*s taken from the cells in ***G*** at 1.2 ms after depolarization (indicated by the dashed line in ***G***) demonstrate that paxilline, but not iberiotoxin, blocked the fast K^+ current completely. ***I***, Monoexponential activation time constants of K^+ currents as a function of voltage for the cells in ***G*** and ***H*** before and during iberiotoxin and paxilline application. Control IHCs without toxin treatment and the iberiotoxin-treated control IHC had time constants of <1 ms. The control IHC treated with paxilline revealed activation time constants of 8 ms (at $\sim$5 mV) that declined to 2 ms (at $\sim$35 mV). ***K***, Voltage-dependent monoexponential activation time constants of K^+ currents for typical control and hypothyroid IHCs of different ages. A P19 control IHC and a P31 hypothyroid IHC displayed fast-activation time constants of $\sim$1 ms or less, whereas P9 control, P9 hypothyroid, P19 hypothyroid IHCs, and a P38 hypothyroid IHC displayed slow activation time constants decreasing from 8 to 10 ms (at $\sim$0 mV) to 2 ms (at $\sim$25 mV). ***L***, IHCs of the same organ of Corti differed regarding the expression of the fast BK conductance in hypothyroid animals aged P31–P50. Selected individual curves of IHC K^+ current activation time constants as a function of membrane potential are shown for three IHCs of a P31 (unfilled symbols) and a P38 (filled symbols) hypothyroid organ of Corti, respectively.

until P11, peak K^+ currents of both groups increased moderately and did not differ from each other. From P11 onwards, K^+ currents of control IHCs showed a steep rise, consistent with the expression of BK channels around and after the onset of hearing, whereas those of the hypothyroid IHCs increased with age at a much lower rate and stayed smaller compared with controls until P30.

To confirm that hypothyroid IHCs lack expression of BK channels, K^+ currents were recorded in response to short (8 ms) step depolarizations, making the differences in activation kinetics more obvious (Fig. 5*A–E*). Whereas the P2 control IHC and the IHCs of the P2 and P19 hypothyroid animals completely lacked any fast K^+ current component ($I_{K,f}$) (Fig. 5*A*,*B*,*D*), rapid currents that were almost fully activated at 1.2 ms after depolarization (Fig. 5*A–D*, vertical dashed lines) were recorded in the control P19 IHC (Fig. 5*C*) and the hypothyroid P32 IHC (Fig. 5*E*). This is also illustrated by the *I–V* curves that were calculated between 1.2 and 1.3 ms after the start of depolarization (Fig. 5*F*).

To directly demonstrate that the BK current underlies the rapidly activating outward K^+ current, we used iberiotoxin, a specific peptide blocker for BK channels (for review, see Meir, 2003). However, iberiotoxin did not block all $I_{K,f}$ of a P18 control IHC, even when superfused at concentrations of 100 nM for 10 min, as shown by the black current traces (Fig. 5G, thick trace, before application; thin trace, after 10 min iberiotoxin application). In contrast, application of 10 μM paxilline, another BK channel blocker (Meir, 2003), inhibited $I_{K,f}$ completely (Fig. 5*G*, gray traces). The differential blocking action of iberiotoxin and paxilline on $I_{K,f}$ in control IHCs is also shown by the *I–V* curves (Fig. 5*H*). On average, 100 nM iberiotoxin blocked 87.7 $\pm$ 8.5% of $I_{K,f}$ at -10 mV ($n = 3$), whereas 10 μM paxilline blocked 100.9 $\pm$ 1.2% ($n = 3$). A block of $>100\%$ indicates that the complete block of $I_{K,f}$ unmasked the small (100 pA) Ca^{2+} inward current. Paxilline unmasked the typical delayed rectifier current in control IHCs, which was similar to those shown in Figure 4, *A*, *B*, and *D*, and had an average peak amplitude of 5.7 $\pm$ 0.8 nA at 0 mV ($n = 3$) (data not shown).

Fitting monoexponential functions to the current traces before and after application of iberiotoxin or paxilline, respectively, revealed that (1) $I_{K,f}$ in control IHCs without any blocker activated with time constants of $\leq$1 ms over the whole voltage range, (2) the iberiotoxin-resistant current was still rapidly activating, albeit slightly slower than the total current, and (3) with paxilline application, only a slow current remained with time constants ranging from $\geq$6 ms at $\sim$0 mV to 2–3 ms at $\sim$25 mV (Fig. 5*I*). These results confirm the heterogeneity of IHC whole-cell BK currents

in the rat that has been described previously for the mouse, where $I_{K,f}$ was composed of an iberiotoxin-sensitive and an iberiotoxin-resistant part, with the latter displaying slightly slower activation kinetics (Marcotti et al., 2004a). They further indicate that the time constant analysis is suitable to test for the presence of BK currents in IHCs. Figure 5*K* shows activation time constants (τ_{act}) of typical IHCs to demonstrate the clear segregation into fast τ_{act} values covered by the mature control IHCs (observed in 13 of 13 IHCs) and slow τ_{act} values covered by P9 control IHCs (five of five), P9 hypothyroid IHCs (four of four), and hypothyroid IHCs aged P19 to P27 (nine of nine). Hypothyroid IHCs aged P28–P75 adopted a dispersed pattern: part of the IHCs gained a conductance nearly as fast as that of control IHCs at P19 (9 of 34) whereas others did not (25 of 34), indicating a delayed acquisition of the BK conductance in part of the hypothyroid IHCs. Interestingly, within one and the same animal, IHCs displaying the fast K^+ current were in direct neighborship of IHCs devoid of the fast current. Figure 5*L* shows activation time constant curves for selected IHCs of two different hypothyroid organs of Corti. In a P31 organ of Corti, two IHCs possessing the BK current and one lacking it were recorded, whereas in a P38 organ of Corti, *vice versa*. The dispersed BK current expression pattern within the same organ of Corti up to P75, but also the apparent lack of BK currents in any IHC tested of two hypothyroid litters at ages P38–P48, underlines the heterogeneity of the hypothyroid phenotype.

The mosaic pattern of BK channel expression was further confirmed using whole-mount immunocytochemistry (Fig. 6). The typical BK channel staining around the IHC neck was seen in each IHC of P30 control rats (Fig. 6*A*). In contrast, in a P35 hypothyroid rat, IHCs were devoid of any BK staining (Fig. 6*B*). At P53, many IHCs of a hypothyroid rat displayed the BK staining around the neck (Fig. 6*C*, filled arrowhead), although some of them were BK negative (Fig. 6*C*, open arrowheads).

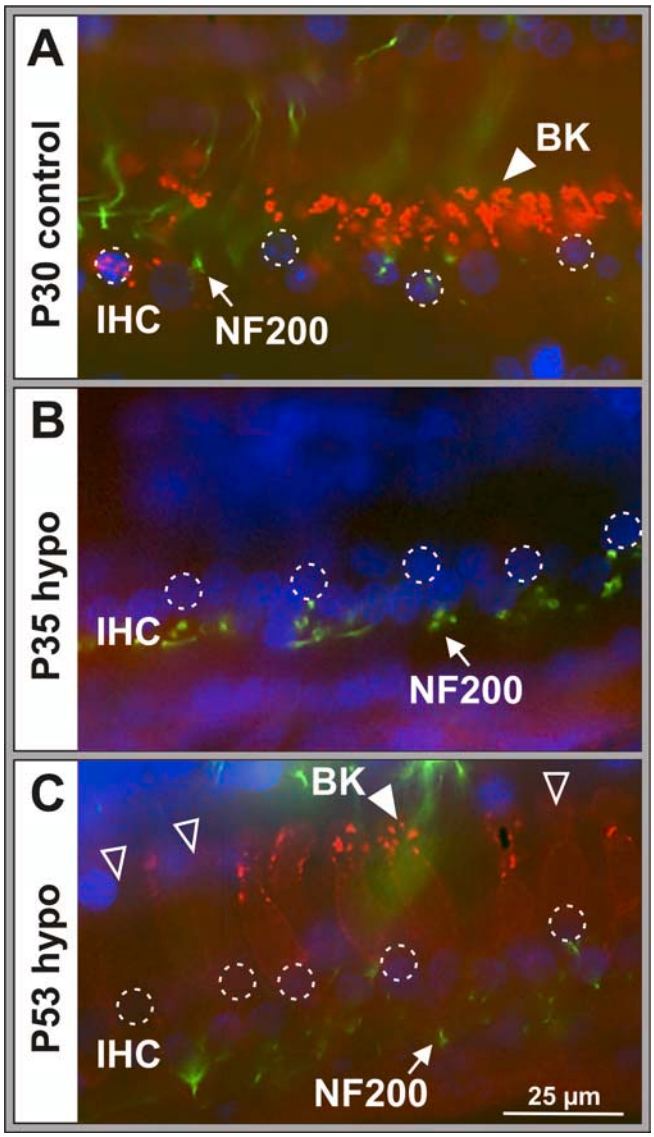

Figure 6. BK channel expression is severely delayed or missing in IHCs of hypothyroid rats. Whole-mount immunocytochemistry on organs of Corti of control and hypothyroid rats was performed with double staining for the BKα subunit (BK, red, closed arrowhead) and neurofilament 200 (NF 200, a marker for afferent fibers, green, arrow). Cell nuclei were stained with DAPI (blue); some of the IHC nuclei are encircled by dashed lines for better orientation. ***A***, Typical patchy BK staining around the neck of control IHCs at P30, medial turn. ***B***, In an organ of Corti of a P35 hypothyroid rat, no BK-positive staining could be detected at the level of the IHCs, here shown for the medial turn. ***C***, In an organ of Corti of a hypothyroid rat at P53, medial turn, BK-positive IHCs were observed, which were, however, less intensively stained compared with the P30 control IHCs (***A***). They were neighboring IHCs that lacked any BK staining (cells are indicated by open arrowheads). Here, the long axis of the IHCs lies in the plane of view, whereas in ***A*** and ***B***, long axes of the IHCs are oriented more perpendicular. The intense blue staining in the top left corners in ***B*** and ***C*** resulted from a greater number of small epithelial cells because of the delayed formation of the inner sulcus caused by TH-deficiency.

Neonatal spiking activity and Ca^{2+} and K^+ currents in athyroid *Pax8*$^{-/-}$ mice

To clarify whether the delays and deficits in IHC maturation observed in hypothyroid rats were independent of the mode of induction of TH deficiency, we analyzed Ca^{2+} APs and currents in athyroid *Pax8*$^{-/-}$ mice and their euthyroid littermates Pax8$^{+/-}$ and Pax8$^{+/+}$ (Christ et al., 2004), further denoted as *Pax8* controls. Within the first postnatal week, IHCs of *Pax8* control and *Pax8*$^{-/-}$ mice generated spontaneous Ca^{2+} APs of similar amplitude and frequency (data not shown). *Pax8* control IHCs had stopped spontaneous spiking at P8, whereas *Pax8*$^{-/-}$ IHCs did so after P14 (Fig. 7*A*). Injection of small positive currents prolonged the period of spiking until P12 in *Pax8* control IHCs and until P21 in *Pax8*$^{-/-}$ IHCs (Fig. 7*B*). Older ages could not be tested in *Pax8*$^{-/-}$ mice because of their death around weaning. Logistic regressions of spiking on postnatal age confirmed later cessation ages in *Pax8*$^{-/-}$ IHCs compared with *Pax8* controls for both spontaneous and induced spiking. Maximum spiking frequencies of *Pax8* control and *Pax8*$^{-/-}$ IHCs were in the range of 5–25 Hz and were not different between the two groups (data not shown).

The presence of Ca^{2+} APs in *Pax8*$^{-/-}$ IHCs in the third postnatal week most likely was attributable to the same reasons as in hypothyroid rat IHCs: failure of downregulation of the Ca^{2+} current and failure of upregulation of the BK current. The central tendency of I_{Ca} was compared between *Pax8* controls and *Pax8*$^{-/-}$ by van der Waerden test, because normality of the small number of values could not be verified. There was a significant ($p < 0.0001$) difference between median I_{Ca}s of *Pax8*$^{-/-}$ and *Pax8* controls (Fig. 7*C*), indicating that I_{Ca} was not downregulated in *Pax8*$^{-/-}$ IHCs. Peak K^+ currents were of similar sizes in neonatal (P2–P4) *Pax8* control and *Pax8*$^{-/-}$ IHCs, indicating that the neonatal delayed rectifier K^+ current was not affected by lack of TH (Fig. 7*D*). Thereafter, average peak K^+ currents became significantly larger in *Pax8* control compared with *Pax8*$^{-/-}$ IHCs [e.g., the K^+ current of *Pax8*$^{-/-}$ was estimated to be 43% (CI, 31 to 58%) of the K^+ current of controls at P16]. This dif-

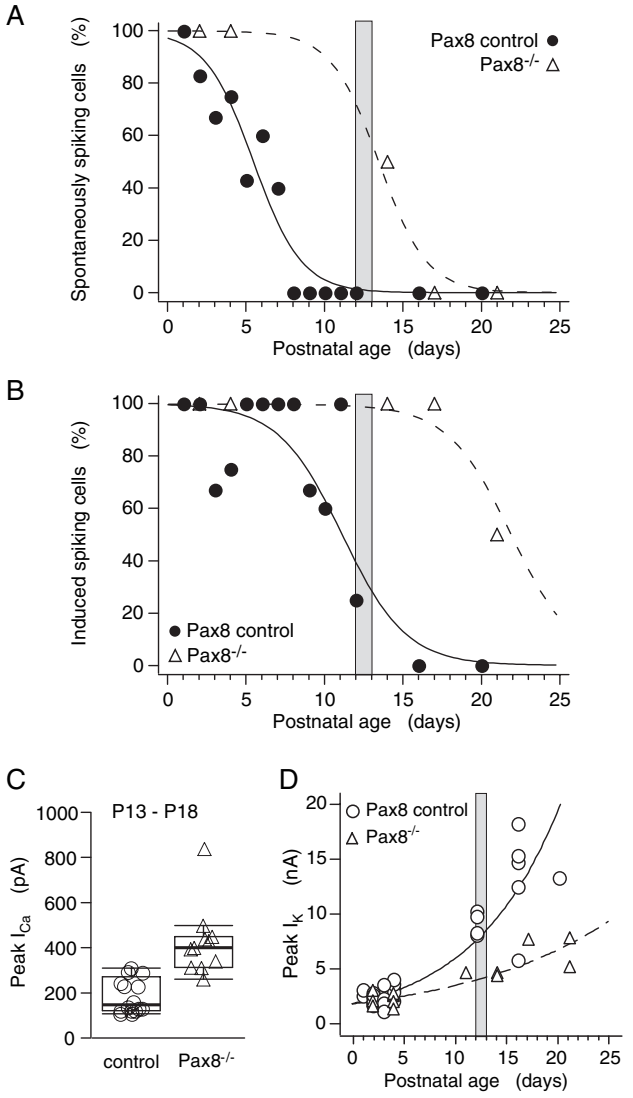

Figure 7. Spontaneous and induced spiking activity persists in IHCs of *Pax8*$^{-/-}$ mice beyond P12 because of changed Ca^{2+} and K^+ currents. ***A***, Percentage of spontaneously active IHCs as a function of age for *Pax8* control and *Pax8*$^{-/-}$ IHCs and logistic fits (solid line, *Pax8* control; dashed line, *Pax8*$^{-/-}$). *Pax8* control IHCs stopped spontaneous activity after P7 whereas *Pax8*$^{-/-}$ IHCs generated Ca^{2+} APs as late as at P14. ***B***, By injecting small currents, Ca^{2+} APs could be elicited up to P12 in IHCs of *Pax8* control mice, but up to P21 in IHCs of *Pax8*$^{-/-}$ animals. Logistic fits are added (solid line, *Pax8* control; dashed line, *Pax8*$^{-/-}$). *n* values: *Pax8* control IHCs, P1, 2; P2, 6; P3, 3; P4, 4; P5, 7; P6, 9; P7, 5; P8, 2; P9, 3; P10, 5; P11, 3; P12, 4; P16, 8; P20, 1; *Pax8*$^{-/-}$ IHCs, P2, 3; P4, 5; P14, 2; P17, 2; P21, 2. ***C***, Box-whisker plot of Ca^{2+} current amplitudes at 5 mM Ca^{2+}; horizontal lines at the median (strong), 25 and 75% quantiles (box), and extreme values within 1.5× interquartile range from the box (whiskers) in 16 *Pax8* controls compared with 11 *Pax8*$^{-/-}$ IHCs aged P13–P18. ***D***, K^+ current as a function of postnatal age for 29 *Pax8* control and 14 *Pax8*$^{-/-}$ IHCs and regressions from logarithms of K^+ currents on postnatal age (*Pax8* control, solid line; *Pax8*$^{-/-}$, dashed line). The gray bars in ***A***,***B***, and ***D*** indicate the approximate age of the onset of hearing in control animals.

ference was caused by the lack of $I_{K,f}$ expression in *Pax8*$^{-/-}$ IHCs at P12 or later, as confirmed by analysis of K^+ current activation time constants and immunohistochemistry (data not shown) (Sendin et al., 2007), similar to our findings for IHCs of hypothyroid rats.

Exocytosis in IHCs of hypothyroid rats and athyroid *Pax8*$^{-/-}$ mice

We demonstrated that IHCs of both animal models of TH deficiency used in this study, hypothyroid rats and *Pax8*$^{-/-}$ mice, show ongoing spiking activity beyond the onset of hearing of their respective controls, when Ca^{2+} APs normally have terminated. Spontaneous activity of IHCs will impair hearing as the transducer current will promote Ca^{2+} APs or lead to an arrest of the IHC in a depolarized state rather than producing graded receptor potentials. We wanted to test whether hypothyroid or athyroid IHCs were able to perform exocytosis at all and, thus, could transmit the aberrant Ca^{2+} AP signaling after P12. Exocytosis (i.e., fusion of synaptic vesicles with the cell membrane) will increase the membrane capacitance. Therefore, capacitance changes were measured in response to voltage steps of varying durations (5–100 ms) from a holding potential of −80 mV to the potential of maximal Ca^{2+} influx (0 mV) for two age ranges in hypothyroid and control rats, at P9 ± 2 d and at P19 ± 2 d (Fig. 8). Figure 8, *A* and *B*, shows current traces in response to depolarizations for 100 ms (top) and the corresponding capacitance changes for P9 and P19 IHCs (bottom). IHCs from hypothyroid and control rats aged P9 showed Ca^{2+} inward currents and ΔC_m values of comparable sizes. For the control IHC, a trace recorded under brief superfusion with a nominally Ca^{2+}-free solution is added, showing very much reduced I_{Ca} and no increase in capacitance (Fig. 8*A*, light gray traces). Prolonged superfusion of the specimen with Ca^{2+}-free solution caused loss of seals and was avoided. In the mature control IHC (P19), depolarization caused a rather small I_{Ca} and smaller ΔC_m compared with the very large I_{Ca} and larger ΔC_m of hypothyroid IHCs (Fig. 8*B*). I_{Ca} inactivation was quite variable and was not different between age-matched hypothyroid and control IHCs (data not shown). We also observed increases of C_m elicited by the high-frequency, 10 mV oscillatory voltage pattern extracted from Fig. 1*E* in hypothyroid IHCs aged 15–18 d at physiological Ca^{2+} concentration (1.3 mM) (data not shown), suggesting that their prolonged spiking activity can be transmitted to the primary auditory neurons.

Figure 8, *C* and *D*, summarizes ΔC_m as a function of duration of the depolarizing stimulus for control and hypothyroid IHCs at P9 (Fig. 8*C*) and P19 (Fig. 8*D*). In general, ΔC_m showed a monotonic increase with the stimulus length for all four IHC groups. At the age of P9, there was no difference in ΔC_m between control and hypothyroid IHCs independent of the stimulus duration (Fig. 8*C*). However, a reduction of ΔC_m was seen in the control IHCs at P19 for depolarizations >20 ms (Fig. 8*D*). In contrast, ΔC_m was markedly elevated in hypothyroid IHCs at P19 compared with P9 (both groups) and to P19 control IHCs (Fig. 8*D*). To analyze the amount of Ca^{2+} that triggered ΔC_m in the different IHC groups, the net Ca^{2+} charge was calculated by integration of the Ca^{2+} current traces for each stimulus duration (Fig. 8*E*,*F*). The net Ca^{2+} influx increased nearly linearly with stimulus duration in control and hypothyroid IHCs of the P9 (Fig. 8*E*) and the P19 group (Fig. 8*F*). For the same stimulus duration, P9 control and hypothyroid IHCs (Fig. 8*E*) and P19 hypothyroid IHCs (Fig. 8*E*) showed a similar Ca^{2+} influx, contrasting the markedly reduced Ca^{2+} influx for stimuli >10 ms in P19 control IHCs (Fig. 8*E*). This confirms the lack of maturation-dependent reduction of the Ca^{2+} current (Beutner and Moser, 2001; Johnson et al., 2005) (Fig. 3*D*).

IHCs normally show an increase in the efficiency of exocytosis during the third postnatal week (i.e., less Ca^{2+} is needed to trigger the same ΔC_m response), which is attributed to the maturation of presynaptic components and a better colocalization of Ca^{2+} channels and ribbon synapses (Beutner and Moser, 2001; Brandt et al., 2005; Johnson et al., 2005; Sendin et al., 2007). Because ΔC_m and I_{Ca} were elevated in hypothyroid compared with control IHCs at P19, we analyzed the efficiency of exocytosis

as membrane capacitance change per net Ca^{2+} influx (Fig. 8*G*,*H*, fF/pC). ANOVA of exocytosis efficiency explained 77% (adjusted R^2) of total variance among the 165 observations on 30 cells. The residual CV was 51% of the respective mean or 37% of random variance. Exocytosis efficiency was a different function of stimulus duration for different combinations of age and genotype (three-way interaction, $p = 0.0066$). Note that the P19 hypothyroid IHCs were similar to both P9 groups (Fig. 8*G*,*H*), suggesting that maturation of presynaptic components or their proper localization was impaired.

The ability to perform exocytosis was tested also in *Pax8*$^{-/-}$ mice. Figure 9*A* shows current traces in response to depolarizations for 100 ms (top) and the corresponding capacitance changes (bottom) for a *Pax8* control and a *Pax8*$^{-/-}$ IHC after P12. The *Pax8*$^{-/-}$ IHC had a threefold elevated Ca^{2+} current but displayed approximately the same amount of ΔC_m compared with the *Pax8* control. Averaged capacitance increases as a function of stimulus duration did not reveal differences between *Pax8*$^{-/-}$ and *Pax8* control IHCs (Fig. 9*B*). The Ca^{2+} influx that triggered these capacitance changes was larger in *Pax8*$^{-/-}$ compared with *Pax8* control IHCs (Fig. 9*C*). Regarding exocytosis efficiency, ANOVA explained adjusted $R^2 = 48\%$ of total variance with a residual CV of 51 or 55% of random variation. The function of exocytosis efficiency on stimulus duration was similar in *Pax8*$^{-/-}$ and control mice ($p = 0.82$), but efficiency of *Pax8*$^{-/-}$ was significantly smaller (59%; $p = 0.0003$) than that of controls (CI, 37 to 73%). Again, this result is in favor of an impaired maturation of presynaptic components or their correct localization under conditions of TH deficiency.

Differences in otoferlin expression in IHCs of hypothyroid rats and athyroid *Pax8*$^{-/-}$ mice

We have shown that hypothyroid IHCs of the rat and athyroid IHCs of *Pax8*$^{-/-}$ mice are able to perform exocytosis in the first three postnatal weeks. A marked difference to control IHCs was, however, the reduced exocytosis efficiency in the third postnatal week, similar to that of neonatal, prehearing IHCs. We therefore analyzed the expression of an IHC protein, otoferlin, which is assumed to play a key role in exocytosis of IHCs (Roux et al., 2006) in hypothyroid rats and *Pax8*$^{-/-}$ mice using *in situ* hybridization and immunocytochemistry. IHCs of *Pax8* control and *Pax8*$^{-/-}$ mice showed otoferlin mRNA in

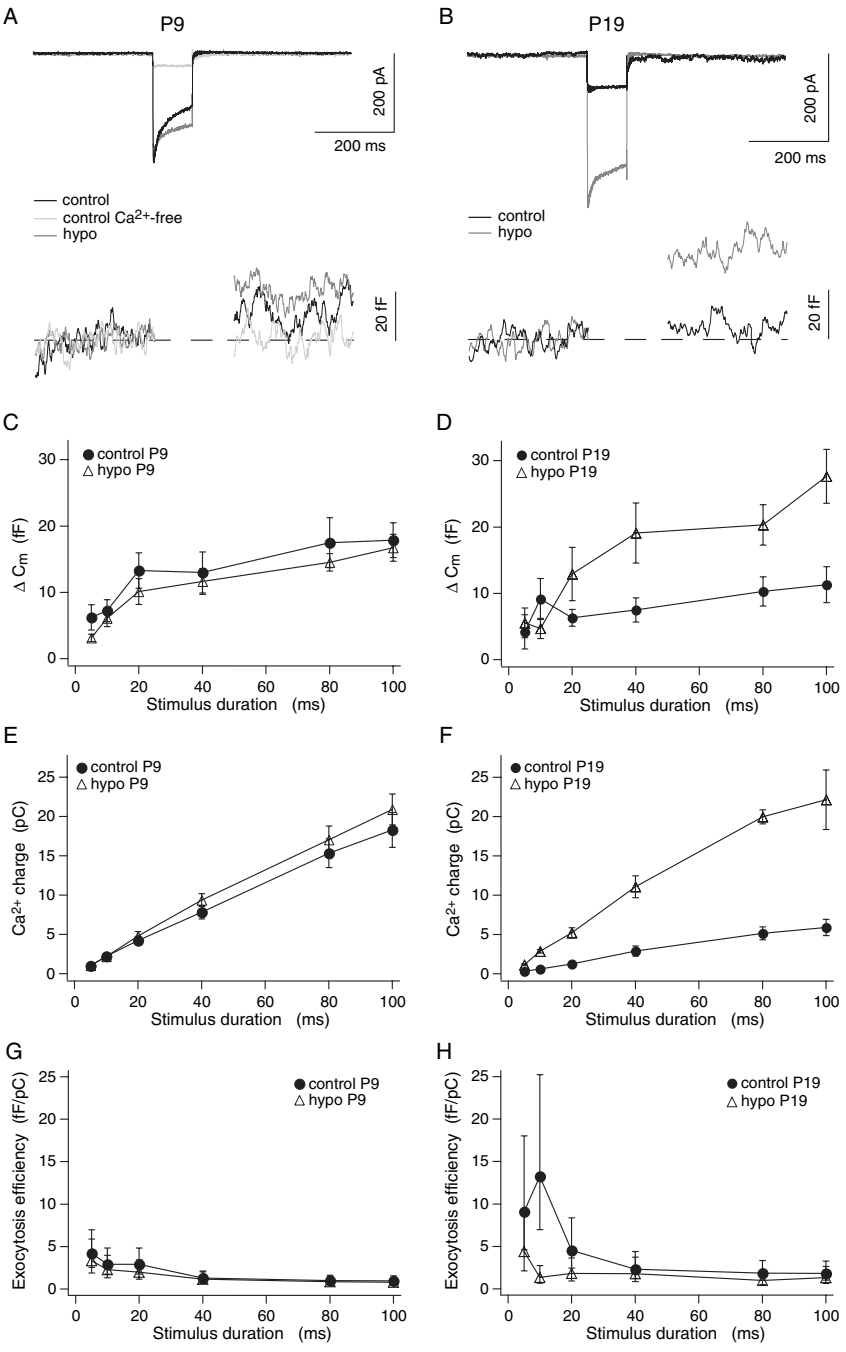

Figure 8. IHCs of hypothyroid rats show exocytosis at both neonatal age and at P19 when IHCs of euthyroid controls are mature. ***A***, Top, Typical Ca^{2+} currents (5 mM Ca^{2+}) of a control (black trace) and a hypothyroid IHC (dark gray trace) in response to depolarizing pulses to 0 mV for 100 ms at P9. The light gray trace shows the residual I_{Ca} in nominally Ca^{2+}-free solution of the control IHC. Bottom, Corresponding increases in membrane capacitance indicate exocytosis in both cells in the presence of Ca^{2+}; zero level is indicated by the dashed line. In Ca^{2+}-free solution, no increase in capacitance was observed. ***B***, Typical Ca^{2+} currents (5 mM Ca^{2+}) of a control (black trace) and a hypothyroid IHC (dark gray trace) at P19 in response to depolarizing pulses to 0 mV for 100 ms (top). Corresponding increases in membrane capacitance indicate larger exocytosis in the hypothyroid IHC compared with the control IHC; zero level is indicated by the dashed line (bottom). ***C***, ***D***, $\Delta C_m \pm$ SEM for control and hypothyroid rat IHCs around P9 (P7–P10, ***C***) and around P19 (P18–P22, ***D***) as a function of the duration of a depolarizing stimulus. P9 control and hypothyroid IHCs showed similar capacitance increases as a function of stimulus duration (***C***). In mature control IHCs, depolarization elicited smaller capacitance increases for depolarization times $\geq$20 ms compared with the age-matched hypothyroid cells (***D***) and the two P9 IHC groups (***C***). ***E***, ***F*** Mean Ca^{2+} charge $\pm$ SEM for euthyroid and hypothyroid rat IHCs around P9 (***E***) and P19 (***F***), respectively, as a function of stimulus duration. Ca^{2+} charges were calculated by integrating the absolute value of the Ca^{2+} current over the time of depolarization. Mature control IHCs showed the smallest influx of Ca^{2+} ions compared with age-matched hypothyroid IHCs (***F***) or with P9 euthyroid or P9 hypothyroid IHCs (***E***). ***G***, ***H*** Geometric means and 95% confidence intervals of exocytosis efficiency as a function of stimulus duration for immature (P9, ***G***) and older (P19, ***H***) control and hypothyroid IHCs. Efficiency of exocytosis was calculated by dividing the capacitance change ΔC_m by the corresponding Ca^{2+} charge. Numbers of IHCs: control, P9, $n = 10$; P19, $n = 7$; hypothyroid, P9, $n = 8$; P19, $n = 5$.

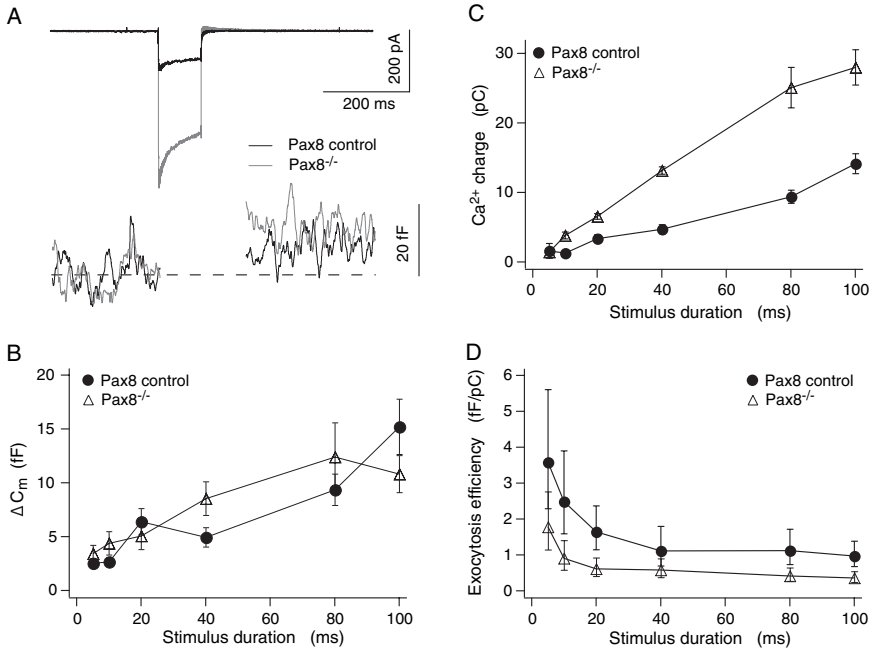

Figure 9. IHCs of athyroid *Pax8*$^{-/-}$ mice display large Ca^{2+} currents and show exocytosis with reduced efficiency. ***A***, Typical Ca^{2+} inward currents (5 mM Ca^{2+}) of a *Pax8* control (black trace) and a *Pax8*$^{-/-}$ IHC (gray trace) in response to depolarizing pulses to 0 mV for 100 ms (top) at P14. Corresponding increases in capacitance indicating exocytosis are shown below; zero level is indicated by the dashed line. ***B***, $\Delta C_m \pm$ SEM for 6–13 IHCs of *Pax8* control and 8–10 IHCs of *Pax8*$^{-/-}$ mice aged P11–P16 as a function of the duration of the voltage pulse. Capacitance increases as a function of stimulus duration were not different for IHCs of *Pax8*$^{-/-}$ animals and *Pax8* controls. ***C***, Corresponding mean Ca^{2+} charge ± SEM for IHCs of *Pax8* control and *Pax8*$^{-/-}$ mice as a function of the duration of the voltage pulse. IHCs of *Pax8*$^{-/-}$ animals showed a larger Ca^{2+} influx for stimulus durations >5 ms. ***D***, Geometric means and 95% confidence intervals of exocytosis efficiency as a function of stimulus duration for *Pax8* control and *Pax8*$^{-/-}$ IHCs.

early postnatal days (P5) (data not shown) and at P12 (Fig. 10*A*). Similarly, otoferlin protein was detected in IHCs of both *Pax8* control and *Pax8*$^{-/-}$ mice in the first postnatal week (data not shown) and around the onset of hearing of *Pax8* control mice (P12) (Fig. 10*B*). The same was true for otoferlin mRNA and protein expression in IHCs of control rats (P9 and P19) (Fig. 10*C–F*, left column), although surprisingly, mRNA and protein were missing in IHCs of hypothyroid rats before (P9) and after (P19) the onset of hearing (Fig. 10*C–F*, right column). These experiments were repeated two times (ISH) and four times (immunocytochemistry) with cochleae of hypothyroid rats of different litters, all yielding the lack of otoferlin on mRNA and protein level, respectively. This unexpected result demonstrates that exocytosis in hypothyroid IHCs of the rat worked without otoferlin and thus questions the crucial role for otoferlin in hair cell exocytosis.

Discussion

The present results indicate that the expression of Ca^{2+} and BK channels in IHCs of mice and rats is TH-dependent. Failure of the downregulation of $Ca_v1.3$ channels and upregulation of BK channels causes persistence of Ca^{2+} APs after P12, the onset of hearing in control animals. Prolonged spiking activity of IHCs could lead to a severe alteration of signals to the brain required for normal functional maturation and for segregation of central neuronal projections.

Altered K^+- and Ca^{2+}-channel expression and persistence of spiking

We observed that TH deficiency affected the expression of the fast activating potassium current $I_{K,f}$ carried by BK channels, a feature similar to what has been described for IHCs of mice lacking TRβ (Rusch et al., 1998). However, in contrast to TR$\beta^{-/-}$ mice in which IHC BK expression was indistinguishable from TR$\beta^{+/+}$ at P50 (Rusch et al., 1998), the phenotype in hypothyroid rats was more severe showing a striking mosaic expression pattern with BK-positive and BK-negative IHCs present in the same organ of Corti even up to P75. Furthermore, activation time constants of BK-positive hypothyroid rat IHCs were slower than in control IHCs, a feature not observed in TRβ mutants. Slower activation kinetics under hypothyroidism may point to an altered molecular composition of BK channels such as altered splice variants of the α subunit or altered assembly with β subunits (Marcotti et al., 2004a).

In the rat, spontaneous spiking lasts from ~P5–P11 whereas in mouse it lasts from before or on P1–P7 (Fig. 7) (Marcotti et al., 2003b). Moreover, the resting membrane potential in neonatal rat IHCs was quite depolarized (−40 to −35 mV) compared with the neonatal mouse (around −60 mV) (Marcotti et al., 2003b). In both species, an abrupt termination of any spiking in control IHCs was observed after P12 whereas Ca^{2+} APs could be evoked in IHCs of hypothyroid rats and *Pax8*$^{-/-}$ mice until P19–P21. Although Kros et al. (1998) proposed the expression of BK channels around P12 as the sole factor for termination of neonatal spiking, evidence is accumulating that there are multiple reasons for AP termination. In light of the previous findings that BK$\alpha^{-/-}$ mice have normal expression of Ca^{2+} and other K^+ (delayed rectifier and KCNQ4-type) currents, show no spontaneous or evoked spiking around P20 (Oliver et al., 2006), and have normal hearing thresholds up to 8 weeks (Ruttiger et al., 2004), it must be concluded that lack of BK neither prevents the termination of spiking nor induces deafness. Instead, two other processes that counteract the generation of Ca^{2+} APs (Muenkner et al., 2002) and occur simultaneously to the termination of spiking in the second postnatal week should be taken into consideration as alternative factors: (1) the downregulation of the Ca^{2+} conductance (Fig. 3) (Beutner and Moser, 2001; Marcotti et al., 2003b) and (2) the expression of a small, very negatively activating K^+ (KCNQ4) conductance that sets the resting potential in mature IHCs (Oliver et al., 2003). The retarded downregulation of the Ca^{2+} conductance in TH-deficient IHCs clearly favors Ca^{2+} APs, similar to the lack of KCNQ4 expression demonstrated in IHCs of *Pax8*$^{-/-}$ mice (Sendin et al., 2007), which, for hypothyroid rats, needs to be confirmed.

Deafness of TRβ mutant mice has been explained as a consequence of the delayed expression of BK channels and, hence, retarded functional maturation of the IHCs (Rusch et al., 1998). The phenotype of BK$\alpha^{-/-}$ mice, which have normal ABR thresholds in the first 8 weeks (Ruttiger et al., 2004), requires that additional deficits in the IHCs or the auditory pathway must be taken into consideration for explaining the severe hearing deficits of TRβ mutants. Here, similar to the observations made in the

present study, the failure of the decline of $Ca_v1.3$ protein leading to increased Ca^{2+} current amplitudes and persistence of Ca^{2+} APs may contribute to their hearing phenotype (see below).

Neuronal consequences of the persistence of Ca^{2+} APs in hypothyroidism

Hair cells mediate the critical function of transducing acoustic stimuli into neural responses. Neurons of the brainstem auditory pathway that extract timing information, such as the octopus or bushy cells of the ventral cochlear nucleus, have strongly differentiating temporal transfer characteristics (Oertel, 1997; Trussell, 1999) and may not develop properly in the third postnatal week if acoustic signal transmission is distorted by the persistent spiking activity of hypothyroid IHCs. Sound-evoked transducer currents would either increase their spiking frequency or lead to an arrest of their membrane potential in a depolarized state. Because the present findings indicate that Ca^{2+} APs of hypothyroid IHCs can trigger exocytosis, deafness of hypothyroid rats, *Pax8*$^{-/-}$ and TR$\beta^{-/-}$ mice may be considered in the context of a critical period for sensory information flow necessary for development of normal hearing (Rusch et al., 1998). Indeed, at least the central effects caused by hypothyroidism may be partly caused by a distorted activity-dependent synaptogenesis in the phase of persisting Ca^{2+} APs that cause aberrant input. Increasing evidence indicates a critical temporal window for the activity-dependent maturation of the auditory cortex (Moore, 1985; Kral et al., 2001, 2002) similar to observations in the visual cortex (Katz and Shatz, 1996). Previously, the critical period for spectral tuning of rat auditory cortex was limited to P9–P14 or later (de Villers-Sidani et al., 2007). However, direct, Ca^{2+} AP-independent effects of TH on the differentiation and functional maturation of neurons in the auditory pathway cannot be excluded (Quignodon et al., 2004). Future studies with a temporally limited suppression of postnatal IHC signaling may give new insights into the role of spontaneous activity for the maturation of the auditory system.

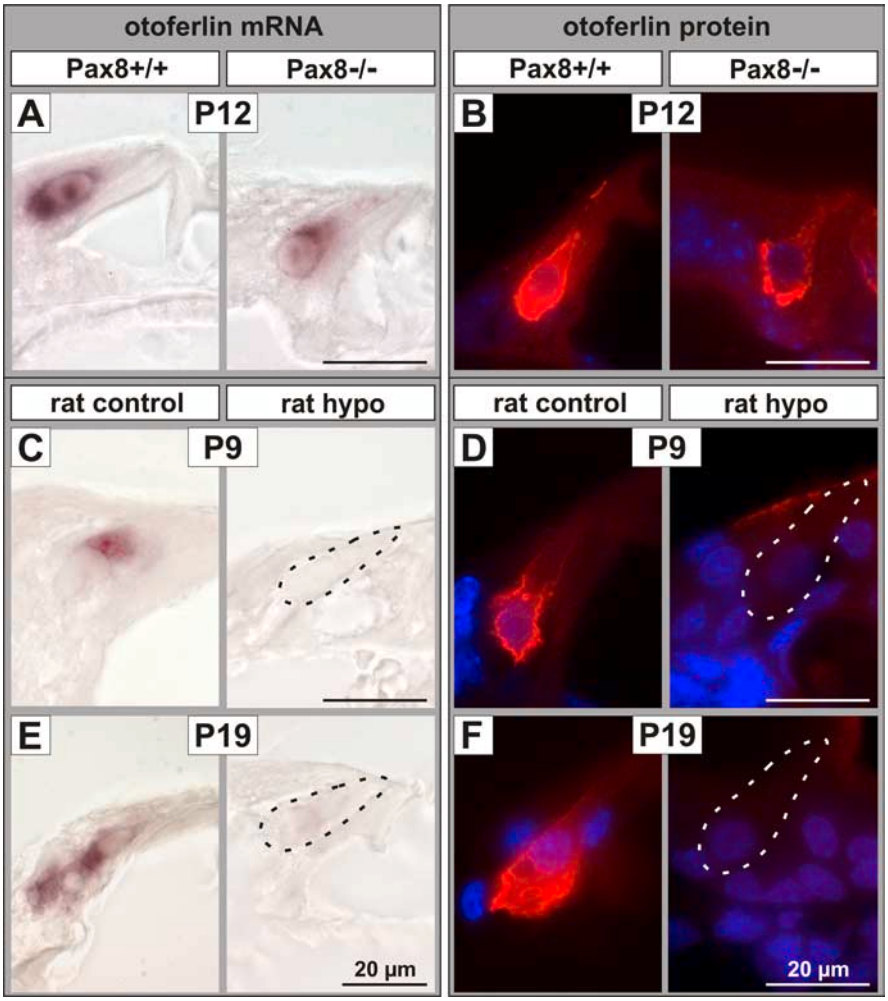

Figure 10. The protein otoferlin is present in IHCs of *Pax8*$^{-/-}$ mice, but not expressed in IHCs of hypothyroid rats. ISH for otoferlin mRNA and immunocytochemistry for otoferlin protein in IHCs in cochlear cryosections of *Pax8* mice or rats. ***A***, ISH of otoferlin mRNA in cochlear sections of a Pax8$^{+/+}$ (left) and a *Pax8*$^{-/-}$ mouse (right) showed antisense hybridization signals in IHCs of both genotypes at P12. ***B***, IHCs of both Pax8$^{+/+}$ (left) and *Pax8*$^{-/-}$ (right) were positively stained for otoferlin (red) at P12. ***C***, ***E***, Otoferlin mRNA present in IHCs of control rats could neither be detected in IHCs of hypothyroid rats at P9 (***C***) nor at P19 (***E***) using ISH. Nonstained IHCs are outlined by dashed lines. ***D***, ***F***, Accordingly, protein staining for otoferlin present in IHCs of control rats at P9 (***D***, left) and P19 (***F***, left) was absent in IHCs of age-matched hypothyroid rats (P9, ***D***, right; P19, ***F***, right; outlines of the IHCs are indicated by dashed lines). In ***B***,***D***, and ***F***, nuclei were stained in blue with DAPI.

Direct and indirect effects of TH

Here, we present a first indication of a negative regulation of the IHC L-type Ca^{2+} channel $Ca_v1.3$ (Platzer et al., 2000) by TH. The question arises if TH affects IHC conductances indirectly or directly through transcriptional effects. To date, only in outer hair cells a direct transcriptional control has been shown for the K^+ channels KCNQ4, BK, and small-conductance Ca^{2+}-activated K^+ channel type 2 (SK2), but not for the Ca^{2+} channel $Ca_v1.3$ (Winter et al., 2006) (H. Winter, C. Braig, and M. Knipper, unpublished observation). The effect of TH on IHCs is different from that on outer hair cells and rather suggests the negative regulation of gene and protein expression of $Ca_v1.3$ and SK2 (C. Braig and M. Knipper, unpublished observation) by increasing TH levels (Flamant et al., 2006). Studies are ongoing to analyze these aspects of transcriptional control.

TH deficiency and exocytosis

IHC Ca^{2+} current amplitudes peak during the short period when most of the IHCs display spontaneous spiking in both rat and mouse (Figs. 2, 3, 7) (Beutner and Moser, 2001; Marcotti et al., 2003b). Considering that neonatal IHC presynapses are not as efficient as mature ones (Beutner and Moser, 2001; Johnson et al., 2005), the large Ca^{2+} amplitude of IHCs around P6 (mouse) or P9–P12 (rat) seems to compensate for the lower efficiency of neonatal exocytosis. The large capacitance increases elicited by voltage pulses of different durations in hypothyroid rat and *Pax8*$^{-/-}$ IHCs were the result of a low exocytosis efficiency that was (over)compensated by a large Ca^{2+} influx (Figs. 8*C–H*, 9*B–D*). P19 rat hypothyroid IHCs performed exocytosis with the same low efficiency as P9 control or P9 hypothyroid IHCs, indicating a lack of presynaptic maturation normally occurring in the

third postnatal week (Beutner and Moser, 2001; Eybalin et al., 2002; Johnson et al., 2005). The reduced exocytosis efficiency (P13–P18) (Fig. 9*D*) (Sendin et al., 2007) and the lack of maturation of presynaptic proteins in IHCs of *Pax8*$^{-/-}$ compared with control mice (Sendin et al., 2007) is in line with this conclusion. Given that in hypothyroid rat IHCs the presynaptic machinery stays similarly immature, the reduced exocytosis efficiency would alone impair hearing thresholds at an age of 4 weeks when Ca^{2+} currents reach the low amplitudes of control IHCs.

Otoferlin is one of the IHC proteins thought to play an essential role in exocytosis (Roux et al., 2006). When mutated, otoferlin causes the human nonsyndromal deafness DFNB9 (Yasunaga et al., 1999, 2000). Unexpectedly, hypothyroid rat IHCs do not express otoferlin mRNA or protein while producing robust capacitance changes, thus, putting into question the indispensable role of otoferlin for IHC exocytosis (Roux et al., 2006).

A lack of otoferlin expression in hypothyroid rat IHCs indicates a regulation of its expression by TH. The striking difference in the phenotype of the athyroid *Pax8*$^{-/-}$ (otoferlin present) versus that of the hypothyroid rat pups (otoferlin lacking) may result from different TH levels in fetal development (Quignodon et al., 2004). Rat fetuses of MMI-treated mothers cannot receive maternal TH whereas *Pax8*$^{-/-}$ fetuses are supplied with a certain amount of maternal TH because their Pax8$^{+/-}$ mothers are euthyroid (Christ et al., 2004). Preliminary data indicating that MMI suppresses otoferlin expression in *Pax8*$^{-/-}$ and *Pax8* control mouse pups (data not shown) are compatible with this view. Although studies are currently underway to clarify this issue, the data nevertheless strongly suggest that otoferlin is not required for immature-like exocytosis. This does however not exclude that otoferlin may be essential for more efficient exocytosis typical for mature IHCs.

References

Beutner D, Moser T (2001) The presynaptic function of mouse cochlear inner hair cells during development of hearing. J Neurosci 21:4593–4599.

Brandt A, Striessnig J, Moser T (2003) CaV1.3 channels are essential for development and presynaptic activity of cochlear inner hair cells. J Neurosci 23:10832–10840.

Brandt A, Khimich D, Moser T (2005) Few CaV1.3 channels regulate the exocytosis of a synaptic vesicle at the hair cell ribbon synapse. J Neurosci 25:11577–11585.

Brucker-Davis F, Skarulis MC, Pikus A, Ishizawar D, Mastroianni MA, Koby M, Weintraub BD (1996) Prevalence and mechanisms of hearing loss in patients with resistance to thyroid hormone. J Clin Endocrinol Metab 81:2768–2772.

Christ S, Biebel UW, Hoidis S, Friedrichsen S, Bauer K, Smolders JW (2004) Hearing loss in athyroid pax8 knockout mice and effects of thyroxine substitution. Audiol Neurootol 9:88–106.

DeLong GR (1993) Effects of nutrition on brain development in humans. Am J Clin Nutr 57 [Suppl 2]:286S–290S.

Deol MS (1973) An experimental approach to the understanding and treatment of hereditary syndromes with congenital deafness and hypothyroidism. J Med Genet 10:235–242.

de Villers-Sidani E, Chang EF, Bao S, Merzenich MM (2007) Critical period window for spectral tuning defined in the primary auditory cortex (A1) in the rat. J Neurosci 27:180–189.

Dussault JH, Ruel J (1987) Thyroid hormones and brain development. Annu Rev Physiol 49:321–334.

Eybalin M, Renard N, Aure F, Safieddine S (2002) Cysteine-string protein in inner hair cells of the organ of Corti: synaptic expression and upregulation at the onset of hearing. Eur J Neurosci 15:1409–1420.

Flamant F, Gauthier K, Samarut J (2006) Thyroid hormones signaling is getting more complex: STORMs are coming. Mol Endocrinol.

Forrest D (1996) Deafness and goiter: molecular genetic considerations. J Clin Endocrinol Metab 81:2764–2767.

Forrest D, Erway LC, Ng L, Altschuler R, Curran T (1996) Thyroid hormone receptor beta is essential for development of auditory function. Nat Genet 13:354–357.

Glowatzki E, Fuchs PA (2002) Transmitter release at the hair cell ribbon synapse. Nat Neurosci 5:147–154.

Hafidi A, Beurg M, Dulon D (2005) Localization and developmental expression of BK channels in mammalian cochlear hair cells. Neuroscience 130:475–484.

Johnson SL, Thomas MV, Kros CJ (2002) Membrane capacitance measurement using patch clamp with integrated self-balancing lock-in amplifier. Pflugers Arch 443:653–663.

Johnson SL, Marcotti W, Kros CJ (2005) Increase in efficiency and reduction in Ca^{2+} dependence of exocytosis during development of mouse inner hair cells. J Physiol (Lond) 563:177–191.

Katz LC, Shatz CJ (1996) Synaptic activity and the construction of cortical circuits. Science 274:1133–1138.

Knipper M, Bandtlow C, Gestwa L, Kopschall I, Rohbock K, Wiechers B, Zenner HP, Zimmermann U (1998) Thyroid hormone affects Schwann cell and oligodendrocyte gene expression at the glial transition zone of the VIIIth nerve prior to cochlea function. Development 125:3709–3718.

Knipper M, Zinn C, Maier H, Praetorius M, Rohbock K, Kopschall I, Zimmermann U (2000) Thyroid hormone deficiency before the onset of hearing causes irreversible damage to peripheral and central auditory systems. J Neurophysiol 83:3101–3112.

Kral A, Hartmann R, Tillein J, Heid S, Klinke R (2001) Delayed maturation and sensitive periods in the auditory cortex. Audiol Neurootol 6:346–362.

Kral A, Hartmann R, Tillein J, Heid S, Klinke R (2002) Hearing after congenital deafness: central auditory plasticity and sensory deprivation. Cereb Cortex 12:797–807.

Kros CJ, Ruppersberg JP, Rusch A (1998) Expression of a potassium current in inner hair cells during development of hearing in mice. Nature 394:281–284.

Langer P, Grunder S, Rusch A (2003) Expression of Ca^{2+}-activated BK channel mRNA and its splice variants in the rat cochlea. J Comp Neurol 455:198–209.

Mansouri A, Chowdhury K, Gruss P (1998) Follicular cells of the thyroid gland require Pax8 gene function. Nat Genet 19:87–90.

Marcotti W, Geleoc GS, Lennan GW, Kros CJ (1999) Transient expression of an inwardly rectifying potassium conductance in developing inner and outer hair cells along the mouse cochlea. Pflugers Arch 439:113–122.

Marcotti W, Johnson SL, Holley MC, Kros CJ (2003a) Developmental changes in the expression of potassium currents of embryonic, neonatal and mature mouse inner hair cells. J Physiol (Lond) 548:383–400.

Marcotti W, Johnson SL, Rusch A, Kros CJ (2003b) Sodium and calcium currents shape action potentials in immature mouse inner hair cells. J Physiol (Lond) 552:743–761.

Marcotti W, Johnson SL, Kros CJ (2004a) Effects of intracellular stores and extracellular Ca^{2+} on Ca^{2+}-activated K^+ currents in mature mouse inner hair cells. J Physiol (Lond) 557:613–633.

Marcotti W, Johnson SL, Kros CJ (2004b) A transiently expressed SK current sustains and modulates action potential activity in immature mouse inner hair cells. J Physiol (Lond) 560:691–708.

Meir A (2003) Large conductance Ca^{2+}-dependent K^+ (BKCa) channels. Target for several pharmacological compounds. Modulator 17:1–3.

Michna M, Knirsch M, Hoda JC, Muenkner S, Langer P, Platzer J, Striessnig J, Engel J (2003) Cav1.3 (α1D) Ca^{2+} currents in neonatal outer hair cells of mice. J Physiol (Lond) 553:747–758.

Moore DR (1985) Postnatal development of the mammalian central auditory system and the neural consequences of auditory deprivation. Acta Otolaryngol [Suppl] 421:19–30.

Moser T, Beutner D (2000) Kinetics of exocytosis and endocytosis at the cochlear inner hair cell afferent synapse of the mouse. Proc Natl Acad Sci USA 97:883–888.

Muenkner S, Engel J, Kros C (2002) Simulating inner hair cells of mice: the BK current suppresses neonatal voltage oscillations. Assoc Res Otolaryngol Abstr 25:62.

Neher E (1992) Correction for liquid junction potentials in patch clamp experiments. Methods Enzymol 207:123–131.

Neher E, Marty A (1982) Discrete changes of cell membrane capacitance observed under conditions of enhanced secretion in bovine adrenal chromaffin cells. Proc Natl Acad Sci USA 79:6712–6716.

O'Malley Jr BW, Li D, Turner DS (1995) Hearing loss and cochlear abnor-

malities in the congenital hypothyroid (hyt/hyt) mouse. Hear Res 88:181–189.

Oertel D (1997) Encoding of timing in the brain stem auditory nuclei of vertebrates. Neuron 19:959–962.

Oliver D, Knipper M, Derst C, Fakler B (2003) Resting potential and submembrane calcium concentration of inner hair cells in the isolated mouse cochlea are set by KCNQ-type potassium channels. J Neurosci 23:2141–2149.

Oliver D, Taberner AM, Thurm H, Sausbier M, Arntz C, Ruth P, Fakler B, Liberman MC (2006) The role of BKCa channels in electrical signal encoding in the mammalian auditory periphery. J Neurosci 26:6181–6189.

Platzer J, Engel J, Schrott-Fischer A, Stephan K, Bova S, Chen H, Zheng H, Striessnig J (2000) Congenital deafness and sinoatrial node dysfunction in mice lacking class D L-type Ca^{2+} channels. Cell 102:89–97.

Pyott SJ, Glowatzki E, Trimmer JS, Aldrich RW (2004) Extrasynaptic localization of inactivating calcium-activated potassium channels in mouse inner hair cells. J Neurosci 24:9469–9474.

Quignodon L, Legrand C, Allioli N, Guadano-Ferraz A, Bernal J, Samarut J, Flamant F (2004) Thyroid hormone signaling is highly heterogeneous during pre- and postnatal brain development. J Mol Endocrinol 33:467–476.

Refetoff S, DeWind LT, DeGroot LJ (1967) Familial syndrome combining deaf-mutism, stuppled epiphyses, goiter and abnormally high PBI: possible target organ refractoriness to thyroid hormone. J Clin Endocrinol Metab 27:279–294.

Roux I, Safieddine S, Nouvian R, Grati M, Simmler MC, Bahloul A, Perfettini I, Le Gall M, Rostaing P, Hamard G, Triller A, Avan P, Moser T, Petit C (2006) Otoferlin, defective in a human deafness form, is essential for exocytosis at the auditory ribbon synapse. Cell 127:277–289.

Rusch A, Erway LC, Oliver D, Vennstrom B, Forrest D (1998) Thyroid hormone receptor beta-dependent expression of a potassium conductance in inner hair cells at the onset of hearing. Proc Natl Acad Sci USA 95:15758–15762.

Ruttiger L, Sausbier M, Zimmermann U, Winter H, Braig C, Engel J, Knirsch M, Arntz C, Langer P, Hirt B, Muller M, Kopschall I, Pfister M, Munkner S, Rohbock K, Pfaff I, Rusch A, Ruth P, Knipper M (2004) Deletion of the Ca^{2+}-activated potassium (BK) alpha-subunit but not the BKbeta1-subunit leads to progressive hearing loss. Proc Natl Acad Sci USA 101:12922–12927.

Sap J, Munoz A, Damm K, Goldberg Y, Ghysdael J, Leutz A, Beug H, Vennstrom B (1986) The c-erb-A protein is a high-affinity receptor for thyroid hormone. Nature 324:635–640.

Schug N, Braig C, Zimmermann U, Engel J, Winter H, Ruth P, Blin N, Pfister M, Kalbacher H, Knipper M (2006) Differential expression of otoferlin in brain, vestibular system, immature and mature cochlea of the rat. Eur J Neurosci 24:3372–3380.

Sendin G, Bulankina AV, Riedel D, Moser T (2007) Maturation of ribbon synapses in hair cells is driven by thyroid hormone. J Neurosci, in press.

Siegel JH, Sikka R, Zeddies DG, Dong Q (2001) Intact explanted adult gerbil cochleae maintained at body temperature. Assoc Res Otolaryngol Abstr 24:858.

Trussell LO (1999) Synaptic mechanisms for coding timing in auditory neurons. Annu Rev Physiol 61:477–496.

Uziel A (1986) Periods of sensitivity to thyroid hormone during the development of the organ of Corti. Acta Otolaryngol Suppl 429:23–27.

Weinberger C, Thompson CC, Ong ES, Lebo R, Gruol DJ, Evans RM (1986) The c-erb-A gene encodes a thyroid hormone receptor. Nature 324:641–646.

Winter H, Braig C, Zimmermann U, Geisler HS, Franzer JT, Weber T, Ley M, Engel J, Knirsch M, Bauer K, Christ S, Walsh EJ, McGee J, Kopschall I, Rohbock K, Knipper M (2006) Thyroid hormone receptors TRα1 and TRβ differentially regulate gene expression of Kcnq4 and prestin during final differentiation of outer hair cells. J Cell Sci 119:2975–2984.

Yasunaga S, Grati M, Cohen-Salmon M, El-Amraoui A, Mustapha M, Salem N, El-Zir E, Loiselet J, Petit C (1999) A mutation in OTOF, encoding otoferlin, a FER-1-like protein, causes DFNB9, a nonsyndromic form of deafness. Nat Genet 21:363–369.

Yasunaga S, Grati M, Chardenoux S, Smith TN, Friedman TB, Lalwani AK, Wilcox ER, Petit C (2000) OTOF encodes multiple long and short isoforms: genetic evidence that the long ones underlie recessive deafness DFNB9. Am J Hum Genet 67:591–600.